AGU PUBLICATIONS
JGR
Journal of Geophysical Research: Earth Surface

RESEARCH ARTICLE
10.1002/2015JF003508

Key Points:
- Elevated, low-relief landscapes were formed in situ in the hinterland of Bhutan
- Landscape reconstructions suggest ~800 m of surface uplift in the hinterland
- Constraints from cosmogenic erosion rates show surface uplift started ~0.8–1 Ma

Supporting Information:
- Readme
- Table S1
- Table S4

Correspondence to:
B. A. Adams,
byron.adams@uni-tuebingen.de

Citation:
Adams, B. A., K. X. Whipple, K. V. Hodges, and A. M. Heimsath (2016), In situ development of high-elevation, low-relief landscapes via duplex deformation in the Eastern Himalayan hinterland, Bhutan, *J. Geophys. Res. Earth Surf.*, *121*, 294–319, doi:10.1002/2015JF003508.

Received 26 FEB 2015
Accepted 30 DEC 2015
Accepted article online 5 JAN 2016
Published online 19 FEB 2016

In situ development of high-elevation, low-relief landscapes via duplex deformation in the Eastern Himalayan hinterland, Bhutan

B. A. Adams[1,2], K. X. Whipple[1], K. V. Hodges[1], and A. M. Heimsath[1]

[1]School of Earth and Space Exploration, Arizona State University, Tempe, Arizona, USA, [2]Now at Department of Geosciences, Universität Tübingen, Tubingen, Germany

Abstract Prior studies have proposed tectonic and climatic mechanisms to explain surface uplift throughout the Bhutan Himalaya. While the resulting enigmatic, low-relief landscapes, elevated above deeply incised canyons, are a popular setting to test ideas of interacting tectonic and climatic forces, when and why these landscapes formed is still debated. We test the idea that these landscapes were created by a spatially variable and recent increase in rock uplift rate associated with the formation of structural duplexes at depth. We utilize a new suite of erosion rates derived from detrital cosmogenic nuclide techniques, geomorphic observations, and a landscape evolution model to demonstrate the viability of this hypothesis. Low-relief landscapes in Bhutan are eroding at a rate of ~70 m/Ma, while basins from surrounding steep landscapes yield erosion rates of ~950 m/Ma, demonstrating that this portion of the range is in a transient period of increasing relief. Applying insights from our erosion rates, we explore the influence of an active duplex on overlying topography using a landscape evolution model by imposing a high rock uplift rate in the middle of a mountain range. Our simulations show that low-relief landscapes with thick alluvial fills form upstream of convex knickpoints as rivers adjust to higher uplift rates downstream, a pattern consistent with geologic, geomorphic, and thermochronometric data from Bhutan. With our new erosion rates, reconstructed paleo-river profiles, and landscape evolution simulations, we show that the low-relief landscapes were formed in situ as they were uplifted ~800 m in the past ~0.8–1 Ma.

1. Introduction

The pattern of mean elevation and local relief within a mountain belt is influenced by spatial and temporal changes in rock uplift rates, the length of transverse tributaries, changes in fluvial dynamics, glacial incision, and spatial patterns of precipitation and rock strength [*Whipple et al.*, 1999; *Whipple*, 2004]. The profile of the eastern Himalaya in Bhutan deviates significantly from the classic profile of the central Himalaya in Nepal, where the lower Himalaya (or foothills) transition to the higher Himalaya (or hinterland) (Figure 1a). Bhutan is generally characterized by a steeply rising mountain front and no abrupt foothills-hinterland topographic transition; instead, isolated, low-relief, high-elevation landscapes in the hinterland interrupt the broader topographic taper (Figure 1a) [*Duncan et al.*, 2003; *Baillie and Norbu*, 2004; *Grujic et al.*, 2006; *Adams et al.*, 2013, 2015]. Because the elevation drop on rivers sets most of the relief in mountain ranges [*Whipple et al.*, 1999], the differences between the mean topography of the Nepal and Bhutan Himalaya are also clearly expressed in the longitudinal profiles of transverse rivers (Figure 1b).

Two primary hypotheses exist for the formation of the enigmatic topography of the Bhutan Himalaya. In the first, surface uplift of low-relief landscapes was caused by a reduction in erosivity, with no change in rock uplift rate, due to a reduction in precipitation rates [*Grujic et al.*, 2006]. In the second, surface uplift of low-relief landscapes was triggered by an increase in rock uplift rate [e.g., *Duncan et al.*, 2003; *Baillie and Norbu*, 2004]. In either case, the presence of high-elevation, low-relief landscapes suggests that landscape adjustment is still in progress, and as knickpoints migrate upstream, local relief will increase and thus eventually increase erosion rates and topographic relief. Interpretation of geochronometric and thermochronometric data suggests that long-term erosion rates and the topography in this portion of the range have been declining since the late Miocene, possibly due to the initiation of new shortening structures in the Shillong Plateau of India to the south that accommodate some of the still-continuing convergence between India and Eurasia [*Coutand et al.*, 2014; *Adams et al.*, 2015] or deformation of the Tibetan Plateau to the north [*Long et al.*, 2012; *McQuarrie et al.*, 2014].

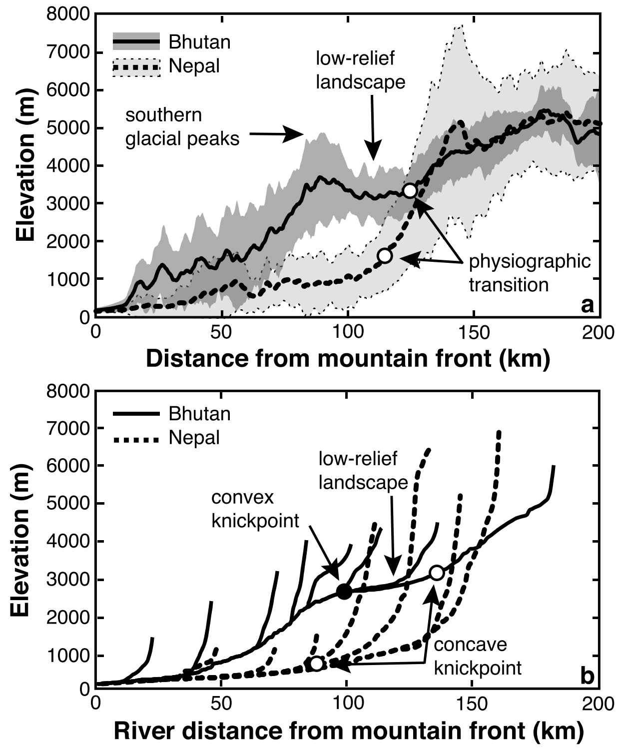

Figure 1. (a) Thirty kilometer wide swath profiles, perpendicular to the strike of the Himalayan range, from central Bhutan and central Nepal (see Figure 2 for locations). Thick lines denote mean elevations and surrounding gray envelopes represent 2 standard deviations about the mean. White dots mark the Physiographic Transition 2 in Nepal and Bhutan. (b) Longitudinal profiles of Himalayan river systems (exclusive of the Tibetan Plateau) within the swath profiles from Figure 1a. The solid black line shows the form of the Chamkhar Chu (CH; Figure 2b) and its tributaries that drain the Bumthang surface of central Bhutan (BS; Figure 2b). The dashed black line shows the form of the Modi Khola and its tributaries that drain the Annapurna region of Nepal. A black dot marks the major convex knickpoint in Bhutan. Note that high glacial peaks are roughly coincident with this knickpoint. White dots mark the concave knickpoints associated with Physiographic Transition 2 in Nepal and Bhutan.

These apparently contradictory hypotheses for the erosional evolution of the Bhutanese sector of the Himalayan orogenic wedge might be reconciled. For instance, if the chronometric data provide evidence for a late Miocene-Pliocene reduction in the thickening of the wedge [*Adams et al.*, 2015], while the geomorphic data provide evidence for a more recent reinvigoration. Thus, geomorphic observation and theory can span the temporal gap between the thermochronometric data and modern day observations. Here we explore this possibility using a combination of methods that builds on thermochronometric constraints on Miocene-Pliocene wedge evolution.

We develop a new conceptual model for the formation of high-elevation, low-relief surfaces in the hinterland of Bhutan from geologic observations, analysis of landforms, and a new detrital cosmogenic radionuclide (CRN) erosion rate data set. We test and illustrate the viability of this conceptual model in simulations using a landscape evolution model [*Tucker et al.*, 2001]. These simulations allow us to develop a strategy to reconstruct paleo-river profiles to calculate the magnitude of surface uplift, which in combination with the detrital CRN erosion rate data allow us to constrain the timing of surface uplift. Given the diversity of approaches required, this paper is organized thematically rather than in a standard method-result-discussion format. After outlining the tectonic setting and context of this study, methods, results and pertinent discussion are incorporated into each thematic section, organized into the following logical progression: (1) morphologic and geologic characterization of the enigmatic high-elevation, low-relief surfaces; (2) description of plausible tectonic models and their diagnostic differences; (3) determination of the spatial pattern of erosion rates (a key diagnostic); (4) hypothesis testing with landscape evolution modeling; (5) determination of the magnitude and timing of surface uplift; and (6) synthesis and discussion.

2. Tectonic Setting

The structural architecture of the Bhutan Himalaya is one of nested tectonostratigraphic packages separated by three major south vergent thrust systems [*Heim and Gansser*, 1939; *Gansser*, 1983]; from the south to north, these are the Main Frontal thrust (MFT), Main Boundary thrust (MBT), and Main Central thrust (MCT) systems (Figure 2a). The active MFT system, which places unmetamorphosed foreland molasse sediments on top of young fluvial sediments and units of the stable Indian craton, is thought to be younger than 5 Ma [*Long et al.*, 2012]. The MBT system, plausibly having a slip history spanning ~10 to 3 Ma [*Long et al.*, 2012], has carried lower amphibolite facies to unmetamorphosed rocks of the Lesser Himalayan sequence over the molasse sequence in the MFT hanging wall. The structurally higher MCT system carries upper amphibolite

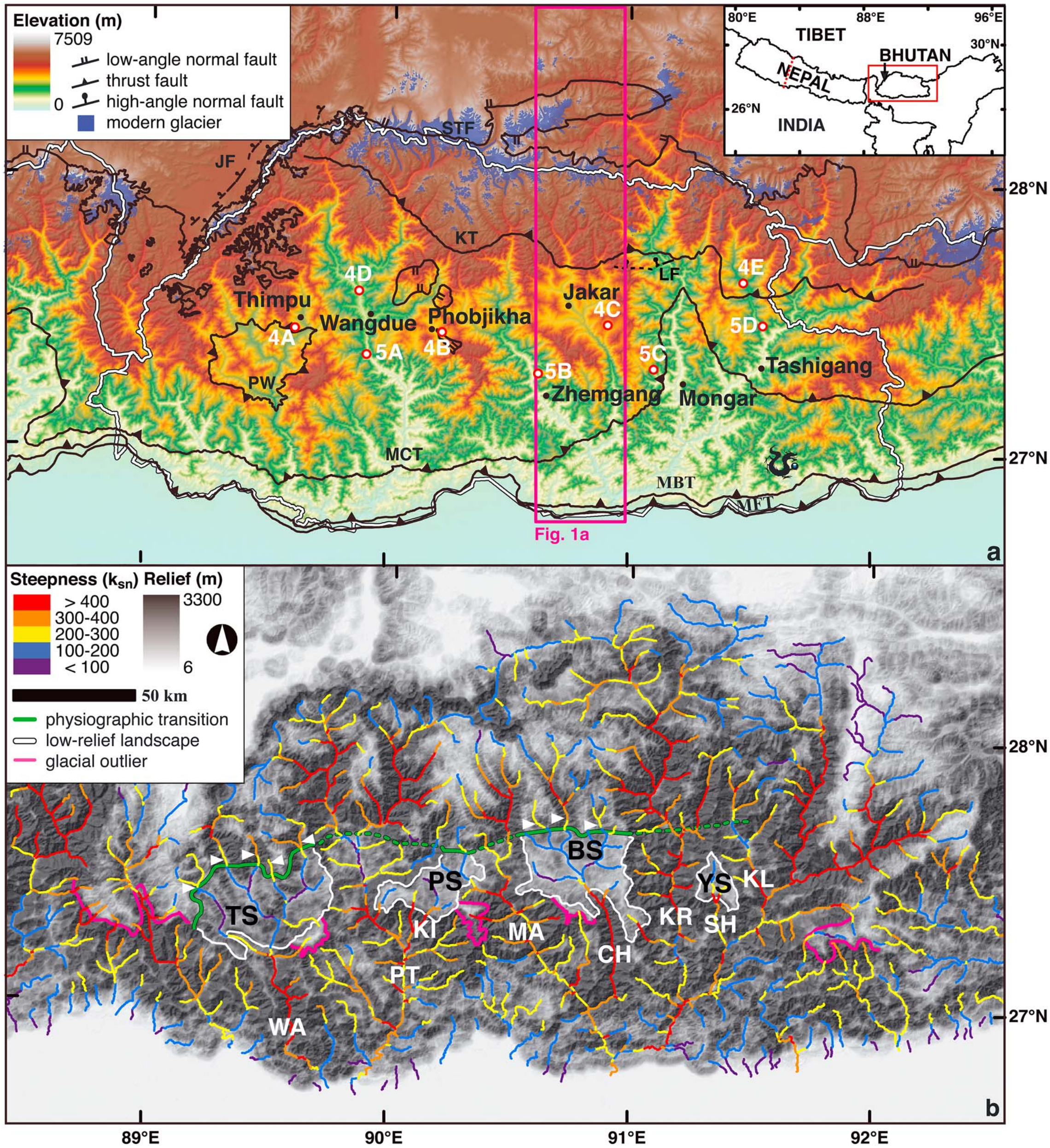

Figure 2. Geography, geology, and geomorphology of Bhutan. (a) Elevation map from 30 m Advanced Spaceborne Thermal Emission Radiometer data. White lines denote the political boarders. Red and white dots mark the locations of the photos in Figures 4 and 5. Magenta box denotes the swath area of data in Figure 1. Red dotted line on inset map is the location of the Nepal swath in Figure 1a. Blue polygons are modern glaciers [*Raup et al.*, 2007]. MFT, Main Frontal thrust system; MBT, Main Boundary thrust system; Main Central thrust system; KT, Kakhtang thrust; STF, South Tibetan fault system; PW, Paro Window; JF, Jomolhari fault system; LF, Lhuentse fault. (b) Local-relief calculated as the range of elevations within a 5 km radius, moving window. The river channels are colored by channel steepness values (see text for description). Green lines mark the location of Physiographic Transition 2. White lines show the extent of the low-relief landscapes. Magenta lines highlight the high, glaciated terrains south of the range crest. Surface names are shown in black: TS, Thimpu surface; PS, Phobjikha surface; BS, Bumthang surface; YS, Yarab surface. River names are shown in white: WA, Wang Chu, PT, Puna Tsang Chu, KI, Kissna Chu, MA, Mangde Chu, CH, Chamkhar Chu, KR, Kuri Chu, SH, Sheri Chu, KL, Kulong Chu. White arrows mark the river reaches north of the low-relief landscapes that were used for profile reconstructions.

to granulite facies units of the Greater Himalayan sequence in its hanging wall. Various researchers have estimated a slip history for this system that began at least 23 Ma and continued until ~10 Ma [*Chambers et al.*, 2011; *Tobgay et al.*, 2012; *Stüwe and Foster*, 2001; *Daniel et al.*, 2003]. In general, the developmental sequence of the MCT, MBT, and MFT systems implies southward propagation of the locus of major thrusting—toward the orogenic foreland—with time, as predicted by the canonical model of orogenic wedge development [e.g., *Davis et al.*, 1983].

However, there are a few known structures that add complexity to the orogenic history of Bhutan. One complication is the Kakhtang thrust [e.g., *Grujic et al.*, 1996], which is located within the Greater Himalayan sequence and strikes broadly subparallel to the MCT system (Figure 2a). The age of Kakhtang thrusting has been estimated as ~14–10 Ma [*Grujic et al.*, 2002], making it an out-of-sequence structure, but the throw on this structure appears to be less than those of the MCT, MBT, and MFT systems. In addition, interpretive geologic cross sections consistent with observed surface geology in Bhutan have led researchers to propose the existence of two major duplex systems resulting in the imbrication of Lesser Himalayan rocks [*McQuarrie et al.*, 2008; *Long et al.*, 2012; *Tobgay et al.*, 2012]. A "lower" duplex is exhumed and exposed at the foreland of the range in the hanging wall of the MBT system. The "upper" duplex is blind (i.e., not exposed at the surface) and positioned under the outcrop extent of the MCT sheet in eastern and central Bhutan [*McQuarrie et al.*, 2008; *Long et al.*, 2012], or beneath other Lesser Himalayan structural packages in western Bhutan [*Tobgay et al.*, 2012; *McQuarrie et al.*, 2014]. While the position, size, and geometry of these duplexes likely vary along the strike of the range, any line of longitude or transverse river in Bhutan is likely to cross at least one major duplex between the range crest and foreland. It was recently suggested that the youngest activity of the upper duplex may date to the middle or late Miocene [*Long et al.*, 2012; *Tobgay et al.*, 2012; *McQuarrie et al.*, 2014] based on geochronometric and thermochronometric data. Invoking upper duplex development as a possible causative mechanism for normal faulting in the hinterland of central Bhutan, *Adams et al.* [2013] suggested that the upper duplex was active in the Quaternary.

Several studies utilizing geochronometry and thermochronometry show that there was a considerable decrease in shortening rates across Bhutan around 9–6 Ma [*Long et al.*, 2012; *McQuarrie et al.*, 2014; *Coutand et al.*, 2014; *McQuarrie and Ehlers*, 2015; *Adams et al.*, 2015]. However, recent GPS studies show that modern shortening rates are 14–17 mm/yr [*Banerjee et al.*, 2008; *Vernant et al.*, 2014], suggesting that rates may have increased again sometime after the 9–6 Ma deceleration. Unfortunately, the youngest thermochronometers are Pliocene in age, which leaves a considerable gap in our knowledge of the evolution of the Bhutan Himalaya.

3. The High-Elevation, Low-Relief Landscapes of Bhutan

Duncan et al. [2003] first noted the belt of high-elevation (~3000 m) terrain with low hillslope gradients and low local relief in the middle latitudes of the Bhutan Himalaya (Figures 1a and 2b) . These low-relief landscapes are found in broad valleys upstream of major convex-up knickpoints (an abrupt downstream increase in channel steepness), and contain thick (perhaps a few hundreds of meters based on the degree of infilling of previously V-shaped valleys), sometimes dissected, packages of sediment. (Following convention, henceforth convex-up and concave-up will be simply refrred to as convex and concave, respectively.) These subdued, filled landscapes were identified within the Thimpu, Bumthang, Phobjikha, and Yarab regions (Figures 2b and 4) [*Baillie and Norbu*, 2004; *Grujic et al.*, 2006]. The abundance of aeolian, colluvial, and alluvial deposits; thick saprolite horizons (>8 m) [*Baillie et al.*, 2004]; and bogs on these low-relief landscapes (Figure 4) suggests very low erosion rates. Large N-S rivers incised deep canyons that isolated these landscapes into smaller patches: the Puna Tsang Chu, Mangde Chu, and Kuri Chu (Figures 2b and 5). Interestingly, despite the considerable relief in these canyons, there are broad, aggraded reaches of the Puna Tsang Chu and Kulong Chu (Figure 3) that are located adjacent to the low-relief landscape patches.

There is no evidence for glacial deposits or glacial modification of topography on these low-relief landscapes. Most cirque and valley glaciers are currently restricted near the crest of the range above 4200 m (Figure 1b) [*Iwata et al.*, 2002]. These glaciers did not advance much in the Holocene and Pleistocene, although some may have reached elevations ~3800 m [e.g., *Iwata et al.*, 2002; *Meyer et al.*, 2009].

Grujic et al. [2006] noted that the Phobjikha, Bumthang, and Yarab surfaces are not correlated with any particular lithology or structure and suggested that they are remnants of an ancient low-relief, low-elevation landscape that was uplifted ~2 km. On the basis of low-temperature thermochronometry, *Grujic et al.* [2006] argued that the mechanism of surface uplift was a reduction in erosional efficiency, brought on by the rain shadow cast by the rising Shillong Plateau to the south, in the presence of constant rock uplift rates. However, *Adams et al.* [2015] suggested that the elevated, low-relief landscapes in Bhutan were more likely formed via a tectonic mechanism. They showed that the Thimpu surface (TS; Figure 2b) is a transient landscape just as the Phobjikha, Bumthang, and Yarab surfaces, despite the fact that it lies to the west of the

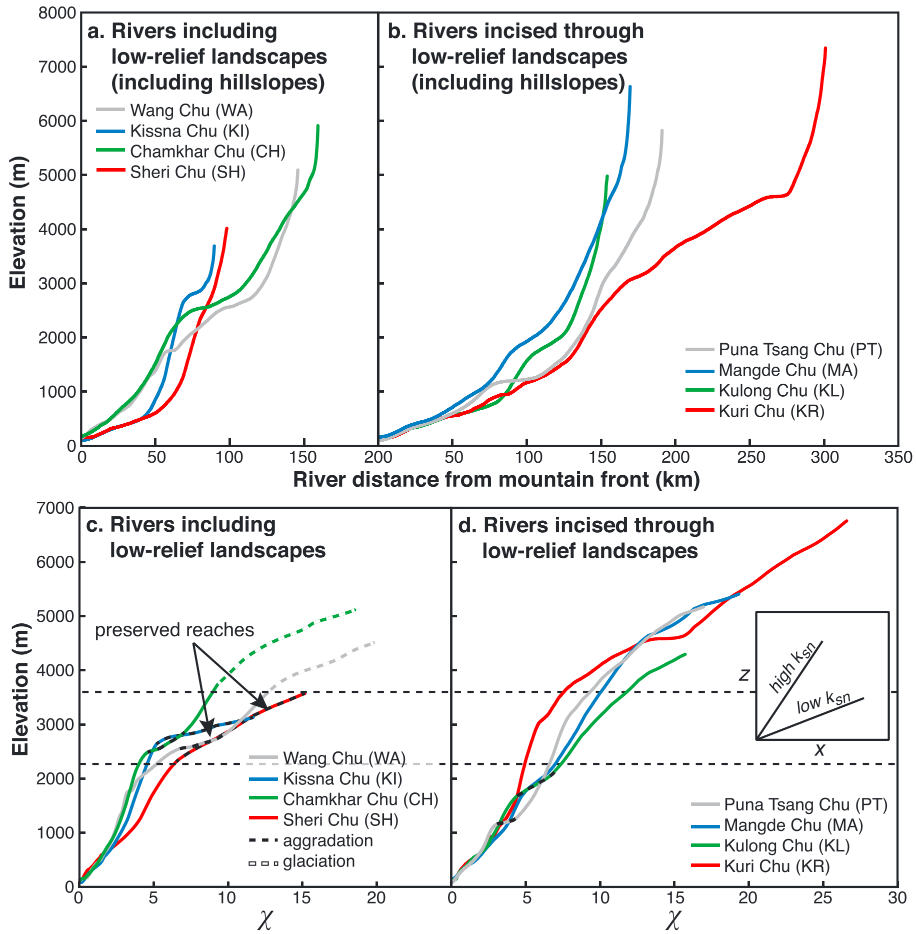

Figure 3. Examples of longitudinal river profiles and linearized channel profiles from the Bhutan Himalaya (see Figure 2b for locations). (a) Longitudinal profiles from the four low-relief landscapes. (b) Longitudinal profiles from the fluvial systems that dissect the low-relief landscapes. (c) Linearized profiles of river from Figure 3a. (d) Linearized profiles of river from Figure 3b. See text for discussion. Reference values used in calculations are $A_0 = 1$ m^2 and $\theta_{ref} = 0.45$. Regions with accumulation areas less that 2 km^2 have been omitted to remove the affects of hillslopes. Slopes of χ plots are the channel steepness values seen in Figure 2b.

supposed rain shadow of the Shillong Plateau. This suggests that the climate change mechanism does not work for all high-elevation, low-relief landscapes in Bhutan. They also used multiple thermochronometers and a thermal-kinematic model to demonstrate that the reduction in erosion rates previously observed [*Grujic et al.*, 2006] was the result of reduced shortening rates in the Bhutan Himalaya, which would not cause surface uplift. *Adams et al.* [2015] were, however, able to deduce that the surface uplift occurred after 3 Ma, and more likely after 1.75 Ma, a condition necessary to preserve the low-temperature cooling ages observed on the surface in Bhutan.

Hodges and Adams [2013] and *Adams et al.* [2013] attempted to simplify the enigmatic topography of Bhutan by separating it into two landforms: (1) the low-relief landscape and associated downstream convex knickpoint and canyons and (2) the higher-gradient topography upstream of these landscapes (Figures 1 and 2b). The transition from the first to the second was referred to in those papers as Physiographic Transition 2 (PT_2) using a terminology originally developed to describe a similar topographic profile in central Nepal [*Hodges et al.*, 2001]. *Hodges and Adams* [2013] suggested that PT_2 in Bhutan might be associated with an active structure generating higher uplift rates to the north like PT_2 in central Nepal [*Wobus et al.*, 2003, 2005, 2006a; *Hodges et al.*, 2004]. *Adams et al.* [2013] did locate a young structure coincident with PT_2 in Bhutan, the Lhuentse fault, but thermal histories of the bedrock north and south of this north dipping fault suggested a normal-sense displacement—opposite the sense required to create the observed step in topography. However, they suggested that the position of PT_2 at the northern edge of the low-relief landscapes could mean that the two had a related formation mechanism related to their hanging wall position above an active duplex structure.

Figure 2b illustrates these observations. We use a map of local relief to highlight the position of the low-relief landscapes across Bhutan as shown by *Adams et al.* [2013, 2015]. We separately identify low-relief regions of high glacial topography to the south of the range crest and adjacent to the southern portions of the fluvial low-relief landscapes. The mean elevations of the glacial surfaces are significantly higher than the fluvial landscapes. As will be discussed in more detail in later sections, we suggest that this is an important designation between fluvial and glacial landscapes, the forms of which are governed by different processes [e.g., *Brozović et al.*, 1997]. The variation in topographic form across Bhutan is also highlighted in a map of channel steepness. Steady state longitudinal river profiles often have a form set by a power law relationship between channel slope and drainage area [e.g., *Hack*, 1957; *Flint*, 1974; *Tarboton et al.*, 1989]:

$$S = k_s A^{-\theta} \tag{1}$$

where k_s is the channel steepness and θ is the channel concavity. Because we found that $\theta = 0.45$ adequately describes the concavity of equilibrium fluvial systems in Bhutan based on regressions of slope-area data, we used that value to normalize measures of local channel slope (S) for the change in upstream drainage area (A) along the length of the channel profiles, and we then calculated a normalized channel steepness (k_{sn}). In this way, we could compare channel gradients for all drainage areas [*Wobus et al.*, 2006b].

Changes exhibited by regional topography are clear from river profile data. In Figure 3 we show longitudinal river profiles as well as linearized profiles. Linearized profiles are shown in χ plots where the profile distance (x) is replaced by a dimensionless term, χ. The integration of equation (1) shows that χ is the integral of the upstream accumulation area (A) [*Perron and Royden*, 2013]:

$$z(x) = z(x_b) + k_s\,\chi \tag{2a}$$

with

$$\chi = \int_{x_b}^{x} \left(\frac{A_0}{A(x)}\right)^{\theta} dx \tag{2b}$$

where x_b is the position of the mouth of the river, A_0 is a reference area ($A_0 = 1\ m^2$ in this study). As indicated in equation (2a), on plots of elevation versus χ, the channel steepness determines the slope of the linearized river profile. Convex and concave knickpoints can be readily identified as positive and negative changes in slope (channel steepness) in these χ plots. Much like the landscapes themselves across Bhutan, profiles of major transverse rivers are highly variable. Every large trunk stream has at least one major convex knickpoint, but these range in style, magnitude, and elevation. The fluvial systems that drain the elevated, low-relief landscapes (e.g., Wang, Kissna, Chamkhar, and Sheri) contain major convex knickpoints that split the basin into two distinct relief regimes (Figures 2b and 3). The very high channel steepness values (likely higher than required by local rock uplift rates, or oversteepened) directly downstream of major convex knickpoints and the low-relief landscapes (Figure 3) make these fluvial systems appear to be on the verge of becoming hanging valleys [e.g., *Wobus et al.*, 2006b; *Crosby et al.*, 2007]. These oversteepened reaches are at least 3 times steeper than surrounding steady state river channels (Figure S1 in the supporting information). Satellite images of the Kissna Chu display sequences of waterfalls downstream of the convex knickpoint.

4. Plausible Mechanisms of Low-Relief Surface Formation

There are two broadly defined tectonic mechanisms that could have created landscapes similar to those observed in Bhutan. The first is a spatially uniform increase in rock uplift rates, perhaps caused by increased fault slip rates of thrust faults near the foreland (e.g., MCT, MBT, or MFT). Such a mechanism would act similarly to that advocated by *Grujic et al.* [2006] in that low-relief surfaces of relict topography formed on grade with the foreland would be uplifted nearly 2 km. Unfortunately, this creates significant problems as the regions to the north of the low-relief landscapes, including the range crest, would have to have experienced ~2 km of surface uplift as well. Such a scenario is highly unlikely as there is no apparent increase in the mean elevation of the range crest or Tibetan Plateau in this portion of the eastern Himalaya. Furthermore, it would suggest that the regions of Bhutan that now appear to be in steady state would have experienced ~2 km of

Figure 4. Examples of the low-relief landscapes and alluvial reaches of otherwise deeply incised valleys (see Figure 2a for locations). (a) Looking north at the city of Thimpu on the Thimpu surface. (b) Looking east on the Phobjikha surface. (c) Looking northwest near the town of Jakar on the Bumthang surface. (d) Looking north at the Punakha Dzong (fortress) on the Puna Tsang Chu. (e) Looking north in the Kulong Chu floodplain north of Tashigang.

exhumation since this change in rock uplift rate. However, such a high amount of exhumation is not permitted by the cooling history of rocks within Bhutan [*Adams et al.*, 2015]. Moreover, this mechanism would not explain the accumulation of valley fill on these low-relief landscapes (Figure 4).

Another mechanism that could explain the in situ production of sediment filled, low-relief landscapes is back-tilting in the hinterland. Such back-tilting could be caused by an antiformal uplift pattern associated with activity on a ramp/duplex structure at depth (e.g., one of the LHS duplexes mentioned above). The deformation of duplex systems at depth result in a pattern of rock uplift similar to that across a generic detachment fold [*Plesch et al.*, 2007], specifically the establishment of an antiform roughly orthogonal to the thrust transport direction.

The response of fluvial systems to increased downstream rock uplift rates has been described for foreland basins [e.g., *Burbank et al.*, 1996; *Humphrey and Konrad*, 2000]. Fluvial systems behave dynamically by aggrading to maintain or change their course, in order to adjust to an impinging zone of higher rock uplift downstream [*Burbank et al.*, 1996; *Wang et al.*, 2014]. The peak of river incision is co-located with the peak of the rock uplift rate, which decreases sharply upstream where rivers must aggrade to maintain a sufficient gradient and counteract the upstream tilting on the back limb of the antiform. This produces a wedge of detritus that propagates upstream as downstream uplift continues. Figure 6 provides an illustration of the predicted patterns of fluvial system response tailored to the landscapes and Late Cenozoic geology of Bhutan described above (section 3).

Uniform and spatially variable rock uplift patterns have predictable erosion rate patterns in portions of the landscape that have completely (or nearly completely) adjusted to the new rock uplift rates. A uniform increase in rock uplift rates would tend to create a uniform increase in erosion rates in portions of the landscapes that have adjusted. However, a spatially variable pattern of rock uplift will lead to spatially variable erosion rates where adjusted portions of the landscape will exhibit higher erosion rates in the presence of higher rock uplift rates. These predictions suggest that either hypothesis could be recognizable from a spatially expansive suite of erosion rate estimates. Cosmogenic radionuclide concentrations in fluvial sands sampled in carefully selected locations can provide the necessary data.

5. Basin-Averaged Erosion Rates

Erosion rates were estimated based on measured concentrations of cosmogenic ^{10}Be in amalgamated quartz sand from modern fluvial systems in Bhutan. This approach is designed to reveal the average erosion rate integrated across a drainage basin [e.g., *Granger et al.*, 1996; *Bierman and Steig*, 1996]. We based our sampling strategy on the hypothesis that some basins in Bhutan are in steady state (or near steady state, as this condition is difficult to demonstrate with 100% certainty), and some are not. Following the protocols established in earlier studies [*Ouimet et al.*, 2009; *DiBiase et al.*, 2010], we identify plausibly steady state basins as those with well-graded channel profiles that are likely eroding all parts of the basin at similar rates (which reflect rock uplift rates). These basins have relatively uniform hillslope gradients, local-relief, and lack major convex knickpoints (Figures S2 and S3). We also sampled basins on the low-relief landscapes that were assumed to be out of equilibrium with modern rock uplift rates. Such landscapes are, instead, likely to be responding to the local baselevel set by the main stem river draining the low-relief landscape patch. Because of this, the basins in these low-relief landscapes are insulated from incised canyons above major convex knickpoints that define local baselevel for the low-relief landscape and were presumed to be eroding well below rock uplift rate (a hypothesis tested in the next sections).

We avoided basins glaciated during the late Pleistocene, and with sediment loads dominated by recent landslides or flood deposits. All sampled catchments lie within the Greater Himalayan sequence, where quartz is ubiquitous at the basin scale, or within quartz-rich portions of the Lesser Himalayan sequence. Basins with upper reaches underlain by Tibetan Sedimentary Sequence rocks were also avoided, as the distribution of quartz in these carbonate-rich units is decidedly nonuniform. As noted earlier, there is a very strong precipitation gradient from south to north in Bhutan created by the effects of orographic precipitation dynamics at the range front (Figure 7). To minimize complicating signals of variable erosivity due to variation in climate, we only analyze here basins from the drier (mean annual rainfall from 0.43 to 1.2 m/yr) interior of the country. The size of the 45 sampled basins ranges from 13 to 274 km^2—large enough to allow an accurate assessment of the channel steepness index (k_{sn}) and to minimize the impact of stochastic landslide contributions to sediment flux [e.g., *Niemi et al*., 2005; *Yanites et al*., 2009; *Kober et al*., 2012], but small enough to sample a single tectonic and topographic terrain.

All samples were processed at the Arizona State University, Surface Processes WOMBAT Laboratory. Quartz grains were separated from the 250–1000 μm fraction of fluvial sands utilizing acid and gravimetric techniques. Sieved sediments were placed in aqua regia at room temperature for 12 h. The samples were then leached in a 5% hydrofluoric and nitric acid solution and rolled on heat for 24 h. Feldspars and micas were floated off using a wetting technique, and dense minerals were removed via heavy liquids. While samples were in heavy liquids special care was taken to separate lighter and denser portions of the quartz fractions to ensure that lithics or crystals with significant inclusions were removed. During the cleaning and separation process, quartz grains were leached at least 5 times with hydrofluoric and nitric acids on heated rollers. These leaching sessions lasted at least 24 h and the final leach lasted for 7 days. The quartz separates were then spiked with ^{9}Be and digested with concentrated hydrofluoric and nitric acids. We removed interfering cations and anions using liquid chromatography techniques. Oxidized beryllium was mixed with a matrix of niobium and loaded into cathodes for analysis on an accelerator mass spectrometer at PRIME Lab, Purdue University. Beryllium isotope ratios were referenced to the isotope ratio standards described by *Nishiizumi et al.* [2007].

5.1. Calculating Basin-Averaged Erosion Rates

We follow the approach of *Portenga and Bierman* [2011] to calculate an effective elevation, latitude, and longitude value that can be used for each sample in the CRONUS online calculator [*Balco et al.*, 2008]. Based on the Advanced Spaceborne Thermal Emission Radiometer 30 m resolution digital elevation data set, we calculated the scaled production rate based on the elevation and latitude of each pixel in a basin. To be internally consistent with the procedures of the CRONUS calculator, we calculated the production rate from spallation reactions using the scheme of *Stone* [2000] and the production rate from muon reactions using the equations of *Heisinger et al.* [2002a, 2002b]. We then calculated the mean of all total production rates (e.g., spallation and muon) within the basin and found the elevation and latitude values corresponding to this mean scaling factor, referred to here as the effective elevation and latitude of the basin. Afterward, we employed the CRONUS calculator to calculate our erosion rates (see Table S1 in the supporting information for CRONUS input data). Because we were not able to adjust the production rate of muons for the erosion rate at each pixel in the basin, it is not accurate to report any time-dependent erosion rate as calculated by the CRONUS calculator. We therefore report erosion rates based on the constant production rates determined by the models of *Lal* [1991] and *Stone* [2000].

5.2. ^{10}Be Basin-Averaged Erosion Rate Results

Our calculated erosion rates vary between ~42 and 2539 m/Ma (Table 1). We estimate the time scales over which these erosion rates integrate by dividing the *e*-folding depth of the penetration of cosmic particles in solid rock (~0.6 m) by the erosion rate. These calculations suggest that our data yield mean rates over at least the last ~0.2–14 ka. The mean erosion rate from the samples collected from the low-relief landscapes is 74 m/Ma with a standard deviation of 24 m/Ma. The mean erosion rate from the surrounding higher relief canyons is 483 m/Ma with a standard deviation of 544 m/Ma.

Our basin-averaged erosion rates reveal a pattern similar to the overall pattern reported by *Portenga et al.* [2015] and *Le Roux-Mallouf et al.* [2015] using the same detrital CRN method. They suggested that latitudinal zones of varying erosion rate could be identified in the Puna Tsang Chu and Wang Chu valleys where a zone of low relief and low erosion rates (27.35°N–27.70°N) is bound by regions of higher erosion rates to the north and south. In the one instance of duplicated sample location from the *Le Roux-Mallouf et al.* [2015] data set, our erosion rates are the same within uncertainty. However, our duplicated basin samples do not always yield the same erosion rates. Of the 49 basins sampled from the Puna Tsang Chu drainage presented by *Portenga et al.* [2015], only 16 met our sampling criteria as described above (others either crossed major knickpoints, incorporated glaciated landscapes, were too small or were too large to sample a single tectonic and topographic zone) (Figure S4). Six of these basins represent duplicate analyses of our samples, of which three are within error of each other. We are not able to explain the disagreement between the other three basin erosion rates—two of our rates are higher and one is lower than those previously published. We ascribe these differences to sampling uncertainty, such as the influx of low ^{10}Be concentration quartz from a flood or mass wasting event, or the addition of high ^{10}Be concentration quartz from the recycling of older terrace deposits. The variability seen in these replicate samples is similar to that observed between samples taken 3 years apart elsewhere in the Himalaya [*Lupker et al.*, 2012; *Scherler et al.*, 2014].

The systematics of possible native ^{9}Be within the samples cannot explain these discrepancies, as the presence of native ^{9}Be would suggest that calculated erosion rates are always too high [*Portenga et al.*, 2015]. In addition, our sample data show a clear relationship between mean basin slope and erosion rate in agreement with that of the sixteen basins from *Portenga et al.* [2015] (Figure S5), adding more compelling evidence that native ^{9}Be has not significantly affected our data set and demonstrating that although sampling uncertainty adds scatter to erosion rate estimates, consistent and robust relationships between erosion rate and controlling variables are reliably obtained. Furthermore, the investigations of *Le Roux-Mallouf et al.* [2015] show that native ^{9}Be is not prevalent in the quartz crystal structure, and any source of native ^{9}Be can be eliminated via targeted laboratory techniques designed to remove inclusions in quartz (see our sample processing procedures above).

The catchments within the low-relief landscapes are eroding much slower than the catchments within the steep flanking terrains (Figures 7 and 8). This pattern confirms that erosion rates on the low-relief landscapes are not reflective of regional rock uplift rates and that the low-relief surfaces are actively being incised and

Table 1. Basin-Averaged Erosion Rate Sample Data

Sample Name	Latitude[a] (°N)	Longitude[a] (°E)	Elevation[a] (m)	Basin Area (km^2)	Channel Steepness (k_{sn})	Channel Steepness 2 SE	Mean Slope (°)	Mean Annual Rainfall[b] (m/a)	[^{10}Be] (atoms/g)	[^{10}Be] 2σ (atoms/g)	Erosion Rate[c] (m/Ma)	Erosion Rate 2σ[c] (m/Ma)	Integration Time[d] (ka)	Used in Calculation[e]
BT0901	27.36735	90.53664	1,083	80	287	33	28	0.71	44,219	11,366	652	194	0.92	C
BT0902	27.33453	90.59394	1,029	132	335	19	29	0.73	39,267	6,460	473	106	1.3	C
BT0903	27.49056	90.52497	2,101	42	227	27	24	0.55	94,955	9,781	208	38	2.9	--
BT0904	**27.49778**	**90.66056**	**2,864**	**48**	**116**	**11**	**20**	**0.49**	**298,794**	**22,003**	**79**	**14**	**7.6**	**--**
BT0905	**27.51247**	**90.65855**	**2,899**	**27**	**109**	**12**	**17**	**0.42**	**475,140**	**43,450**	**47.8**	**8.8**	**13**	**--**
BT0906	**27.49453**	**90.66548**	**2,875**	**30**	**107**	**12**	**20**	**0.49**	**200,487**	**33,450**	**117**	**27**	**5.1**	**--**
BT0907	**27.49517**	**90.66873**	**2,871**	**110**	**107.2**	**7.0**	**18**	**0.43**	**261,393**	**36,444**	**89**	**19**	**6.8**	**--**
BT0909	**27.62447**	**90.87717**	**2,785**	**65**	**155**	**16**	**23**	**0.64**	**336,625**	**52,665**	**74**	**16**	**8.1**	**--**
BT0910	**27.62046**	**90.89055**	**2,777**	**57**	**153**	**16**	**18**	**0.61**	**351,628**	**41,298**	**72**	**14**	**8.4**	**--**
BT0912	**27.66471**	**90.90198**	**2,865**	**50**	**193**	**24**	**24**	**0.60**	**243,388**	**23,907**	**115**	**22**	**5.2**	**--**
BT0922	**27.61051**	**90.67154**	**2,735**	**114**	**168**	**12**	**19**	**0.46**	**311,891**	**52,989**	**80**	**19**	**7.5**	**--**
BT0926	27.47798	91.18580	930	59	356	42	28	0.59	97,598	10,294	168	31	3.6	--
BT0927	27.50703	91.18533	1,045	21	353	94	28	0.57	170,952	10,500	88	14	6.8	--
BT0928	27.55829	91.20886	1,071	53	345	60	30	0.60	85,463	5,555	191	31	3.1	--
BT0929	27.68762	91.17019	1,240	13	396	325	31	1.2	95,408	7,138	131	22	4.6	--
BT0931	27.71488	91.15016	1,278	91	248	12	31	1.0	79,985	6,700	215	37	2.8	--
BT0973	**27.44027**	**90.96384**	**3,444**	**20**	**54.9**	**8.5**	**16**	**0.45**	**642,631**	**42,777**	**41.6**	**7.2**	**14**	**--**
BT0993	27.52560	89.86707	1,440	114	188.3	8.9	23	0.82	165,244	20,205	134	26	4.5	--
BT0994	27.66848	89.77	1,372	108	274	13	29	0.97	16,682	3,124	1130	273	0.53	--
BT0995	27.45604	89.90343	1,190	74	233	37	26	0.64	109,994	9,685	132	23	4.5	--
BT0996	27.29762	89.96644	750	41	239	38	28	0.83	54,706	7,519	318	62	1.9	W
BT0998	27.26743	90.04733	696	65	237	14	34	0.92	26,354	16,802	736	531	0.82	W
BT09108	**27.43180**	**89.68176**	**2,355**	**42**	**166**	**14**	**23**	**0.77**	**318,378**	**29,411**	**65**	**12**	**9.2**	**--**
BT1021	27.72669	91.14786	1,283	71	313	36	28	0.74	170,813	26,434	193	42	3.1	--
BT1036	**27.32944**	**89.48227**	**2,203**	**37**	**201**	**14**	**23**	**0.63**	**701,376**	**60,009**	**45.0**	**8.1**	**13**	**--**
BT1042	**27.42643**	**90.10416**	**2,918**	**37**	**98.5**	**8.6**	**21**	**0.69**	**548,906**	**83,564**	**65**	**14**	**9.2**	**--**
BT1043	**27.41452**	**89.99476**	**2,595**	**57**	**105**	**12**	**18**	**0.76**	**563,798**	**127,285**	**53**	**15**	**11**	**--**
BT1044	27.76806	89.72473	1,714	89	377	36	29	0.55	68,274	10,073	644	138	0.93	--
BT1111	27.29421	90.01186	846	26	239	11	33	0.69	4,611	1,152	2539	738	0.24	W
BT1112	27.26769	90.02112	672	89	210	10	29	0.75	16,405	1,290	692	112	0.87	W
BT1135	27.22863	90.64284	930	85	265	19	32	1.1	10,710	1,530	1343	275	0.45	C
BT1142	27.56014	90.44263	2,127	45	181	23	23	0.85	129,722	10,902	135	23	4.4	--
BT1143	27.54067	90.44250	1,956	15	206	32	23	0.76	168,089	11,837	98	16	6.1	--
BT1145	27.28870	91.23264	1,047	45	209	18	25	0.60	76,555	4,927	148	23	4.1	--
BT1146	27.38511	91.20358	783	48	307	47	31	0.85	18,065	2,038	756	139	0.79	E
BT1147	27.51644	91.17115	934	274	268	12	30	0.78	65,403	4,557	252	42	2.4	--
BT1148	27.66405	91.43760	1,898	52	235	14	24	1.1	64,367	3,773	306	50	2.0	--
BT1149	27.61926	91.48538	1,770	14	212	7.2	26	1.1	154,680	9,276	103	17	5.8	--
BT1150	27.58434	91.49039	1,630	94	215	10	26	0.83	103,263	5,670	179	29	3.4	--
BT1151	27.55414	91.52150	1,709	22	257	31	27	0.97	97,374	5,180	166	26	3.6	--
BT1152	27.40153	91.54840	1,162	34	252	18	30	0.64	49,382	3,407	244	39	2.5	--
BT1153	27.34473	91.62375	968	56	299	26	27	0.91	26,856	3,292	574	110	1.0	E
BT1154	27.35791	91.67211	1,038	66	286	22	26	0.83	10,401	1,431	1541	312	0.39	E
BT1161	**27.47549**	**90.35015**	**2,386**	**29**	**162**	**36**	**17**	**0.81**	**187,988**	**19,019**	**102**	**19**	**5.9**	**--**
BT1162	**27.43434**	**89.68533**	**2,387**	**56**	**146.2**	**9.5**	**22**	**0.72**	**285,871**	**24,423**	**69**	**12**	**8.7**	**--**

[a]Actual sample location data. See Table S1 for CRONUS input data.
[b]Twelve year average, mean annual rainfall calculated from Tropical Rainfall Measuring Mission 2B31 data set [*Bookhagen and Burbank*, 2010].
[c]Values calculated using the CRONUS calculator and the constant prodution rate model of *Lal* [1991]/*Stone* [2000].
[d]Time over which the erosion rate is integrated. This value is calculated by dividing the *e*-folding depth of the production of cosmic nuclides via spallation (0.6 m) by the erosion rate.
[e]This denotes which erosion rates where used in the calculation of surface uplift timing from different transects: W = western, C = central, E = eastern. Bold samples are located within low-relief landscapes.

erased as river reaches downstream steepen to erode at higher rates, and knickpoints migrate headward. Erosion rates of the higher-relief catchments are highest near the southern margins of the low-relief landscapes adjacent to high, isolated glacial terrains (~27.2–27.4°N), and decrease to the north. The northern tributaries in the Puna Tsang Chu also exhibit high erosion rates and channel steepness values; however, this pattern is only based on two data points. There is also no strong correlation between erosion rates and rainfall across Bhutan (Figure 8).

Since erosion rates are generally set by rates of rock uplift relative to baselevel [e.g., *Whipple and Tucker*, 1999], we interpret our map of erosion rates in catchments not part of low-relief landscapes as a map of rock uplift rates, which suggests that the rock uplift rate pattern is nonuniform in Bhutan, and likely highest in the middle latitudes (~27.2–27.4°N). Importantly, not all of the basins flanking the low-relief landscapes are equally steep nor eroding at similar rates, which would be expected from a scenario involving a simple increase in regional rock uplift rate. These findings also imply that higher rock uplift rates in the middle latitudes of the range may have promoted the development of high terrain such as the abundant glacial landscapes flanking the low-relief landscapes, and near the western and eastern borders of Bhutan. Taken together, these observations suggest an antiformal pattern of rock uplift rate such as might be associated with growth of a duplex stack at depth [*Boyer and Elliott*, 1982] (see Figure 2). To test our hypothesis that the topography of Bhutan may be adjusting to an antiformal uplift pattern, we turn to a landscape evolution model.

6. Landscape Evolution Modeling

We used the Channel Hillslope Integrated Landscape Development Model (CHILD) landscape evolution model [*Tucker et al.*, 2001] to explore how fluvial systems in mountainous landscapes respond to the onset of an antiformal uplift consistent with duplex deformation midway between the crest of a range and the range front. The results of our model experiments are heuristic and illustrative to simply test the hypothesis that rock uplift and landscape back-tilting associated with the onset of duplex deformation could produce landforms analogous to the high-elevation, low-relief, landscapes in Bhutan. We do not seek a best fit model to constrain a full suite of model parameters that most completely explain the topography of Bhutan. Instead, we only focus on developing systems analogous to the Chamkhar and Wang rivers that developed low-relief, aggradational surfaces upstream of major convex knickpoints with oversteepened reaches downstream (Figures 1–5). Beyond evaluating whether the back-tilt hypothesis is plausible to explain (1) the formation of high-elevation, low-relief landscapes, (2) the wedges of sediment accumulation characteristic of these landscapes, (3) the chain of high, glaciated peaks along their southern margins, and (4) the enigmatic physiographic transition that marks their northern boundaries, we do not use the model results quantitatively. Rather, rates magnitude, and timing of Bhutanese landscape evolution are addressed independently using a combination of topographic analysis and detrital cosmogenic radionuclide erosion rates informed and guided by the landscape evolution models and presented in later sections.

To model landscape response to blind duplex growth, it is necessary to represent river incision into bedrock, as well as the transport and deposition of the sediment load, which generally precludes simple 1-D profile evolution models. It is also important that as convex knickpoints continue to migrate upstream (both laterally and vertically), the model be able to simulate the erosion of weak, recently deposited, river gravels. The simplest model that meets these requirements is the mixed or hybrid detachment and transport model [e.g., *Whipple and Tucker*, 2002]. We have configured the CHILD model to run in this mode as described in the next sections.

The formation and maintenance of major convex knickpoints and hanging valleys have been investigated using nonlinear incision models based on the availability of river gravels (tools) or their overabundance (cover) [e.g., *Gasparini et al.*, 2007; *Crosby et al.*, 2007]. While we infer that the oversteepening of large rivers draining low-relief landscapes is a manifestation of the lack of tools in response to simultaneous downstream steepening and upstream trapping of gravels in piggyback basins, we suggest, based on prior experience with such models, that current implementations of tools versus cover river incision models are incapable of effectively capturing the complexity and scale of the Bhutan landscape. Thus, we choose to work with simpler models and to focus on the question of low-relief surface formation at the scale of our larger low-relief landscapes. We return to this topic in the discussion of our model results.

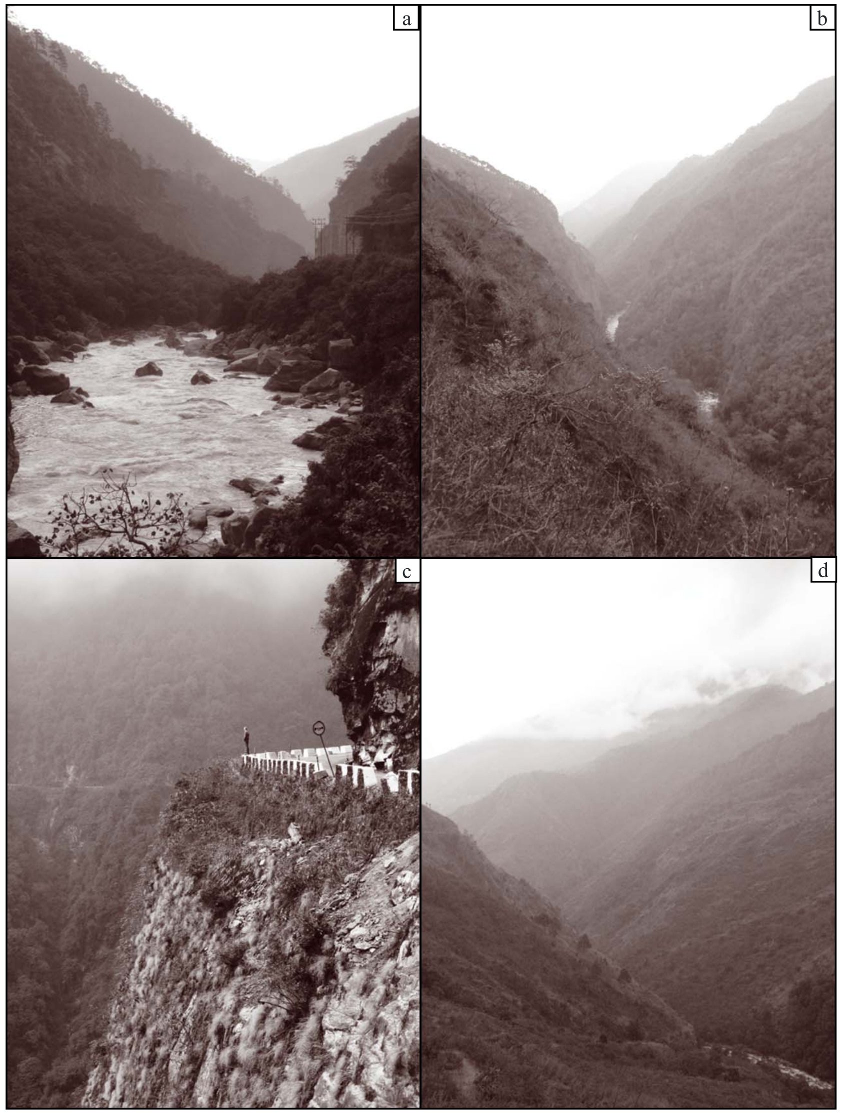

Figure 5. Examples of the deep canyons that dissect low-relief landscapes in Bhutan (see Figure 2a for locations). (a) Looking south (downstream) on the Puna Tsang Chu, south of the town of Wangdue. (b) Looking south (downstream) on the Mangde Chu north of the town of Zhemgang. (c) Looking northwest in a tributary basin of the Kuri Chu northwest of the town of Mongar. (d) Looking north (upstream) on the Kulong Chu north of the city of Tashigang.

6.1. Model Formulation

In mixed or hybrid mode, CHILD tracks the evolution of surface elevations using the conservation of mass:

$$\frac{dz(x,y)}{dt} = U(x,y) - E(x,y) \tag{3}$$

where $z(x,y)$, $U(x,y)$, and $E(x,y)$ are the spatial patterns of elevation (m), rock uplift rate relative to baselevel (m/yr), and erosion rate (m/yr) (defined as positive downward—where deposition is negative erosion). The erosion rate, $E(x,y)$, is dictated by either detachment of bed material or the divergence of the sediment flux, whichever predicts the slower, and thus limiting, rate. With this formulation, erosion rates are determined as detachment-limited incision whenever volumetric sediment transport capacity, Q_c (m^3/yr), exceeds volumetric sediment flux, Q_s (m^3/yr), and as transport-limited erosion or deposition whenever $Q_c \leq Q_s$ [e.g., *Whipple and Tucker*, 2002].

In our experiments detachment-limited incision was computed using the well-known stream power incision model [e.g., *Howard and Kerby*, 1983; *Whipple and Tucker*, 1999]:

$$E = K_b Q^{m_b} S^{n_b}. \tag{4}$$

where K_b is the bedrock erodibility coefficient (here K_b has the units of m^{1-3mb} yr^{mb-1}) Q is the water discharge (m^3/yr), S is the channel slope (m/m), and m_b and n_b are dimensionless constants, held fixed at 0.5 and 1, respectively, in our experiments. A value of 0.5 for the m_b/n_b ratio is consistent with the findings of channel shear stress river incision models and observed steady state channel concavity [e.g., *Whipple and Tucker*, 1999]. When previously deposited sediments (tracked and termed "regolith" in CHILD) are incised under detachment-limited conditions ($Q_c > Q_s$) a higher detachment coefficient, referred to as K_r with subscript r denoting erosion of regolith rather than bedrock, is used because these are more easily eroded. Under transport-limited conditions, fluvial erosion, E, was calculated as the downstream divergence of the sediment flux [e.g., *Willgoose et al.*, 1991; *Tucker and Bras*, 1998]:

$$E = \frac{dQ_c}{dA} \tag{5a}$$

where

$$Q_c = K_f Q^{m_f} S^{n_f} \tag{5b}$$

K_f is the sediment transport coefficient (here K_f has the units of m^{3-3mf} yr^{mf-1}), and m_f and n_f are dimensionless constants held fixed at values of 1.5 and 1, respectively, following *Whipple and Tucker* [2002], again to approximate typically observed concavities of steady state or graded channels [e.g., *Tucker and Whipple*, 2002]. K_f was assigned the same value as K_r in our experiments, to ensure consistent river profiles during aggradation or sediment re-incision, and to ensure that discrete convex knickpoints developed during transient channel-profile adjustment to an increase in rock uplift rate (i.e., detachment-limited incision would prevail at steady state and during a response to renewed or accelerated rock uplift), as observed in Bhutan.

At steady state ($E = U$), channel slope, S, increases monotonically with rock uplift rate relative to baselevel, regardless of whether incision is detachment-limited or transport-limited such that

$$S = \left(\frac{U}{K'}\right)^{\frac{1}{n'}} A^{-\theta'} \tag{6}$$

where $K' = K_b$ (or K_r if incising regolith), $n' = n_b$, and $\theta' = m_b/n_b$ if incision is detachment-limited, and $K' = K_f$, $n' = n_f$, and $\theta' = (m_f-1)/n_f$ if incision is transport-limited [e.g., *Whipple and Tucker*, 2002]. Equation (6) is analogous to equation (1); the first term on the right-hand side of equation (6) is the channel steepness index (k_s).

In our modeling experiments, we used a value of $5e^{-6}$ for the erosion coefficient of bedrock (K_b) and $5e^{-5}$ for the erosional coefficient of regolith (K_r), and transport coefficient of sediment (K_f). Using equation (6), it becomes clear how the order of magnitude difference between our chosen coefficients will affect the topography within our models. For a given basin of a certain size (A) and rock uplift rate (U), the channel slope will scale inversely with the coefficients (K'). Therefore, river reaches that are incising into regolith, or those that are transport limited, will be 10 times less steep than reaches that are detachment limited.

6.2. Experimental Setup and Initial Steady State Landscape

Experiments were performed on a 30 × 30 km, regular triangular lattice of 250 m node spacing, with a southern open boundary. In our experiments, an antiformal uplift pattern was imposed upon a steady state landscape. To create the initial landscape, we assumed uniform regional uplift (1 mm/yr) of a random topography described by a mean elevation of 10 m and a standard deviation of 0.5 m, and we allowed the landscape to evolve until a steady state topography associated with uniform channel steepness and erosion rate was reached (Figure 9a). At steady state, this landscape was in a detachment-limited condition. A selection of longitudinal river channel profiles of varying lengths illustrates the smooth, concave profiles with uniform channel steepness values (Figure 9b). In this landscape, fluvial relief scales with catchment size and thus increases steadily toward the crest of the modeled mountain range (Figure 9b).

6.3. Imposing an Active Duplex

It is well known that fault-bend folds associated with simple thrust faults or those with multiple blind splays (horses), as is the case in a duplex, create an antiformal rock uplift pattern [*Suppe*, 1983]. Such patterns have been measured in the Siwalik mountains of the central Himalaya. The work of *Lave and Avouac* [2000] produced a detailed assessment of the rock uplift gradient associated with the MFT in central Nepal. That gradient was a peaked function with a broad apex and was significantly skewed toward the foreland. Without knowing the exact position, size, or geometry of an active blind duplex in Bhutan, we chose a similar, simple, geologically reasonable geometry. The pattern of uplift above the duplex was modeled as a strike-parallel, 20 km wide, triangular (isosceles) ridge. The front limb was pinned to the southern edge of the landscape. Uplift rates increased linearly toward the crest on each limb of the duplex. Figure 9c shows the duplex uplift pattern that we applied to our initial steady state topography. This antiformal geometry was chosen as a conservative end-member of possible uplift patterns. More extreme end-member conditions could include broader spatial patterns of high rock uplift or sharper gradients (e.g., stepped changes). However, such rock uplift patterns would only act to perturb river incision patterns more aggressively. North of the back limb of the duplex is a 10 km wide section of the landscape that was uniformly uplifted at the same rate as the base of the duplex (U_l), which was set equal to the initial uniform rock uplift rate such that the only perturbation to the steady state landscape was the increase in uplift rate above the modeled duplex.

The maximum uplift rate at the crest of the duplex (U_h) was varied between 1.5 and 8 times greater than the initial, background uplift rate (U_l). This range of U_h/U_l ratios spans a reasonable range of expected spatial changes in vertical rock uplift rates due to the spatial variability in rock transporation vectors. For example, if the regional rock uplift rate is controlled by transportation over a 4° dipping basal décollement [*Long et al.*, 2011] and 16° dipping structures within duplexes, then we could expect a fourfold change in the regional rock uplift gradient regardless of the slip rate (see Table S2 for more details).

Although there is some evidence for orders of magnitude differences between K_b for intact bedrock and K_r for weakly indurated sedimentary sequences [*Stock and Montgomery*, 1999], the channel steepness across boundaries where channels switch from eroding bedrock channels to depositing alluvial channels often decreases only by a factor of 2–10 in Bhutan (e.g., across PT_2 and at the front of the range). As our models are not importantly sensitive to $K_{f/r}/K_b$ ratios (see Table S3), we use the intermediate value of 10 (a high-end estimate from observations in Bhutan, a and low-end estimate from previous studies [*Stock and Montgomery*, 1999]) as a representative value in the model runs presented here.

The model run with $U_h = 4U_l$ and $K_{f/r} = 10K_b$ was selected for illustration (Figure 10) as this condition effectively created convex knickpoints separating steep, rapidly eroding downstream reaches from aggradational upstream reaches, but was not so severe as to tectonically defeat rivers and cause drainage reversal [e.g., *Sobel et al.*, 2003]. We emphasize that the $K_b/K_{f/r}$ and U_h/U_l ratios used in our modeling are reasonable values but are not unique to the process of forming elevated, low-relief landscapes, nor do these ratios necessarily quantitatively describe conditions in Bhutan. The degree to which landscapes similar to observations in Bhutan form depends on the relative values of these two ratios (see Table S3 for experiment parameters tested). However, we find that our models were most sensitive to the U_h/U_l ratio, whereby it is difficult to produce significant low-relief landscapes at high $K_b/K_{f/r}$ ratios (e.g., 100) when U_h/U_l ratios are less than 3. Rock uplift ratios of greater than 5 tend to defeat and reverse drainage patterns regarless of the $K_b/K_{f/r}$ ratio. We present the above values as they permit the formation of convex knickpoints and sediment wedges upstream, similar to actual observations in Bhutan, as will be documented below.

6.4. Landscape Response to an Active Duplex

Figures 10a–10c show the initial response of our experimental landscape to the onset of active duplex deformation. The elevations of mountain peaks near the crest of the duplex have increased, and deep canyons with higher channel steepness values have formed. All channel reaches on the front limb of the duplex and a few on the back limb have remained detachment-limited. Local relief has increased greatly near the crest of the duplex and decreased in parts of the back limb and behind the duplex. However, the local relief near the back of the modeled landscape has not changed because the rivers are still detachment-limited and the rock uplift rate relative to baselevel has not changed (Figure 10c, Profile 1).

The map of erosion rates exhibits a similar pattern, but only a small fraction of the landscape has adjusted to a new erosion rate set by higher rock uplift rates. Figure 10b shows focused incision in the front limb near the crest of the duplex. However, in the back limb deposition is prominent, as rivers adjust to the new high rock uplift rate downstream by raising their bed elevations via aggradation. Failure to match the rising local base-level set by the migrating knickpoints with a similar deposition rate would have led to a defeated, ponded river and an internally drained basin [e.g., *Humphrey and Konrad*, 2000].

River profiles within the front limb of the duplex have steepened, and fluvial relief has increased (Figure 10c). Convex knickpoints have formed in the longitudinal profiles of channels that cross the crest of the duplex. As the knickpoints migrate headward they move vertically, and set the rate of baselevel rise upstream. These knickpoints also track an important boundary between detachment- and transport-limited reaches within the landscape. The vertical movement is associated with continued surface uplift created by disequilibrium of erosion rates and rock uplift rates upstream of the knickpoint. The surface uplift rates of landscapes vary as a function of the rock uplift rate at the position of the convex knickpoints as the knickpoints migrate laterally relative to the nonuniform rock uplift pattern. Larger basins that extend to the back of the model also develop transient concave knickpoints where upper detachment-limited river reaches aggrade and become transport-limited (Figure 10c, Profile 1). The landscape created by this dichotomy in local relief and fluvial character associated with these concave knickpoints generates a subtle physiographic transition to gentler slopes and local relief downstream.

Figures 10d–10f show further response of our experimental landscape. The development of low-relief landscapes has continued behind the crest of the duplex, and detachment-limited channel reaches behind the duplex have nearly disappeared. However, convex knickpoints have migrated farther upstream into the back limb and have removed thick packages of sediment that were previously deposited. The elevation of mountain peaks and local relief has increased in the front limb and near the crest of the duplex. The region near the foreland has eroded rapidly, but the landscapes behind the crest of the duplex have been dominated by active deposition.

The sediment wedge that formed from continued deposition has migrated farther upstream, and thus, the concave knickpoint and associated physiographic transition have moved headward. This knickpoint migration decreased the area of steeper landscapes above the low-relief landscape and has made it difficult in these models to resolve the associated physiographic transition. Surface uplift has continued, but the magnitude of surface uplift, and therefore the elevation of convex knickpoints, is not the same for all rivers. The magnitude of surface uplift is greater for rivers with convex knickpoints that remained close to the crest of the duplex, as the rock uplift rate is greater at these positions. Fluvial relief no longer simply increases from the front to the back of the modeled landscape, and large peaks near the crest of the duplex have reached similar elevations as the former steady state range crest of the modeled landscape.

6.5. Model Comparison With Bhutan

The goal of our landscape evolution model experiments was to evaluate whether the key topographic characteristics of Bhutan could be created by an antiformal uplift pattern. Therefore, the patterns—more than absolute values, of channel steepness, mean elevation, and local-relief in the simulated landscapes—are the most useful metric to compare to the observed patterns of landscape morphology in Bhutan. We monitored the pattern of channel steepness because this metric contains information regarding the state of the river (i.e., if it is in, or out of equilibrium), the uplift rate it is experiencing, and its channel incision regime (i.e., K'). Despite not directly attempting to reproduce the evolution of the Bhutan Himalaya, our modeled landscape is similar in form, except for the lack of deeply incised canyons interspersed between aggraded, elevated valleys across the strike of our synthetic mountain range. The modeled landscape exhibits high mountain peaks much closer to the front of the range coincident with the region of highest uplift rate at the crest of the duplex. These high peaks are interpreted as analogous to the regions of glaciated peaks outboard of the Himalayan crest in Bhutan. To the north of the high peaks, the modeled landscape is filled with fluvial sediments and local relief has been reduced. This is very similar to our observations of the low-relief landscapes of Bhutan. A pattern of high-to-low-to-high channel steepness and local relief, from the front to the back of the model, has developed much like that observed in Bhutan. The southern transition (high-to-low channel steepness and local relief) marks the position of transient convex knickpoints in the model and in Bhutan. The northern transition (low-to-high channel steepness and local relief) marks the position of a transient concave knickpoint in the model and in Bhutan (e.g., PT_2).

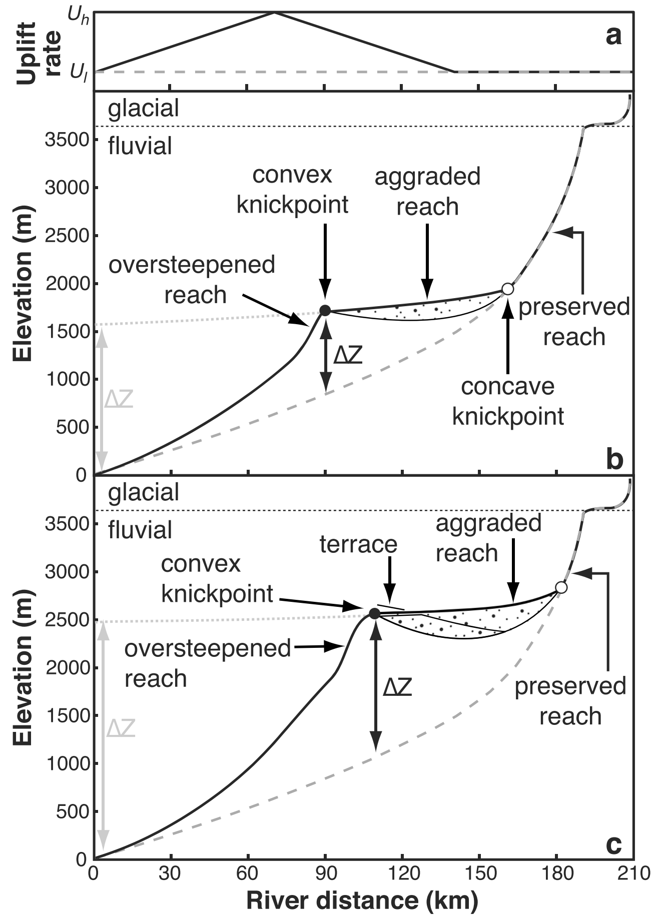

Figure 6. Cartoon cross section showing the evolution of a hinterland landscape affected by a downstream zone of high rock uplift rate. Dashed gray line shows the initial river profile before duplex activity (when uniform uplift was equal to the lower uplift rate U_l). The black line denotes the shape of the perturbed river profile after (a) the nonuniform rock uplift rate pattern was imposed. The stippled pattern marks the packages of sediment accumulating upstream of a migrating convex knickpoint (black dot) and forming the migrating concave knickpoint upstream (white dot). Portions of the original fluvial landscape are preserved between the concave knickpoint and glacial terrains. The magnitude of surface uplift (ΔZ) can be easily calculated as the greatest difference between the former and current river profile. This magnitude calculated in this way (black markers) is much smaller than if the aggraded reaches are extrapolated to the foreland of the range (gray markers). (b) Landscape soon after duplex activation. (c) Landscape long after duplex activation. Note that older packages of sediment are cut and rotated as duplex activity continues. The upper discontinuity in the profile is created by glacial incision. U_h, high uplift rate at the crest of the duplex.

Armed with these observations from our experimental landscape, morphometric analysis, field observations, and new erosion rate map, we have developed a new conceptual model for the formation of the low-relief landscapes of the Bhutan Himalaya. Figure 6 shows a cartoon of this conceptual model and highlights a few key points. First and foremost, the low-relief landscapes of Bhutan are not relicts of an uplifted portion of the Himalayan foothills [e.g., *Grujic et al.*, 2006]. This means that the magnitude of surface uplift cannot be measured by assuming the low-relief landscapes once graded to the current elevation of the mouth of the river at the foreland of the range. Second, the idea behind this new conceptual model implies that the best method for calculating the magnitude of surface uplift is measuring the difference between the modern river profile and the profile of the paleo-river projected from the modern river reaches upstream of the low-relief surfaces at the position of the convex knickpoint (ΔZ in Figure 6). Estimates of surface uplift based on projections of the low-relief surfaces themselves would lead to a gross overestimate.

7. Magnitude and Timing of Surface Uplift

7.1. Quantifying Surface Uplift

To calculate the magnitude of surface uplift (the total rock uplift since surface uplift initiation, minus the total erosion on the main stem river crossing the uplifting landscapes since surface uplift initiation), we reconstructed the form of river profiles that reflect the landscape before surface uplift occurred, and then calculated the difference between the paleo-river profiles and the modern river profiles. We conducted our paleo-river reconstructions by projecting existing river reaches downstream using the relationship between drainage area and channel gradient along an upstream segment that has preserved the presurface uplift form [e.g., *Schoenbohm et al.*, 2004]. Our method utilized the simplicity of χ plots to make straightforward linear regressions and extrapolations of preserved river reaches. We predict new elevation values for the downstream reconstructed river based on the channel steepness (the slope of the χ plot). We report the amount of surface uplift as the difference between the modern linearized river profile (z versus χ) and the reconstructed linearized profile at the position of the convex knickpoint (Figure 11). Because inherent quantitative errors associated with our elevation or χ data are minimal we evaluated the uncertainty in our surface uplift calculation based on the scatter in our elevation and χ data. This was achieved by using a jackknife technique where a random subset of our preserved reach data was used in each regression. The number of data pairs used in each regression was equal to the square root of the total number of pairs in the preserved reach, which yields a rigorous assessment of the scatter. We report the magnitude of surface uplift for each preserved river reach as the mean and 2 standard deviations of 10,000 jackknifed regressions.

To produce the most accurate reconstructions of the rivers of Bhutan, we selected channel reaches within regions not apparently affected by recent rock uplift change, aggradation, or glaciation (Figure 3). Comparisons with our landscape evolution model and the observed sediment deposits both suggest that the low-relief landscapes of Bhutan were actively aggrading as they adjusted to the local baselevel rise created by a migrating convex knickpoint and are therefore not useful for reconstruction of paleo-river profiles. Thus, we restricted the downstream extent of reaches selected for analysis to upstream of the concave knickpoints found at the physiographic transition to the north of the low-relief landscapes (Figure 2b). As the Lhuentse fault may lie at or near the concave knickpoints at the northern boundary of the low-relief landscapes, we took special care to avoid the use of these reaches for our reconstructions. Of the four elevated, low-relief landscapes highlighted in this study, the Yarab and Phobjikha surfaces could not be reconstructed due to lack of suitable upstream river reaches. Therefore, we focused our river profile reconstructions on the channels of the Thimpu and Bumthang surfaces (Figure 11).

The magnitude of surface uplift each low-relief landscape experienced was calculated as the weighted mean surface uplift value of multiple tributary profiles within that landscape. Uncertainties on the mean values were calculated by propagating the individual uncertainness (described above) through the weighted mean calculation in quadrature, and then multiplying this value by the square root of the mean square weighted deviation to account for external uncertainties [see *Wendt and Carl*, 1991]. The mean surface uplift magnitudes from the Thimpu and Bumthang surfaces are 870 ± 90 m (2σ, five tributaries) and 748 ± 56 m (2σ, three tributaries), respectively.

The slight difference in magnitude may be due to variability in rock uplift rate along strike of the duplex, noise within the elevation data used to define each river reach, or the degree to which selected reaches faithfully record presurface uplift channel profiles. It is also important to note that the pattern of surface uplift along each profile cannot be simply interpreted as a spatial distribution in rock uplift rate. The difference between the modern profile and a reconstruct profile is a function of the rock deformation at the position of the convex knickpoint, minus the erosion rate at that point, but upstream of this position the surface uplift rate is the sum of the rock uplift rate and the deposition rate. In this case, the pattern of rate of rock uplift upstream of the knickpoint cannot be known without constraints on the deposition rate and geometry of the fill.

7.2. Timing of Initiation of Surface Uplift

While independent thermochronometric data constrain the recent phase of surface uplift to no earlier than 3 Ma [*Adams et al.*, 2015], our river profile reconstructions and detrital CRN erosion rates can be used to derive a more precise estimate of the timing of young surface uplift, and thus the timing of inferred duplex deformation. We used the definition of the magnitude of surface uplift given by the conservation of mass (equation (3)):

$$\Delta Z = t(U - I) \tag{7}$$

where U is the rock uplift rate, I is the incision rate into bedrock at the position of the migrating convex knickpoint, and t is the duration of surface uplift. We assumed that the high-relief basins adjacent to the low-relief landscapes have adjusted to a new rock uplift rate (as illustrated in the landscape evolution simulations in Figure 10) and substituted the rock uplift rate with the erosion rates in the canyons yielding:

$$t = \Delta Z(E - I) \tag{8}$$

where E is the characteristic erosion rate in the deep canyons near the convex knickpoint. Although I will be nonzero in the early stage of the landscape response, the incision rate into bedrock at the position of the knickpoint (within the back-tilted zone) has been effectively zero for most of the duration of surface uplift. This condition is created by active deposition upstream of the rising knickpoint, and the resulting protection of the bedrock channel until the instant that the knickpoint migrates past a given location and re-erodes the alluvial deposits. As such, equation (8) can be further simplified by setting $I = 0$, and we can use our estimates of surface uplift magnitude and rock uplift rate in the vicinity of the major convex knickpoints to calculate our best estimates of the initiation of surface uplift along each of our transects (Figure 8). The mean uncertainty of our erosion rates is 20% (2σ) of the rate. We apply a more conservative 30% (2σ) uncertainty for estimates of E

and propagate these and the uncertainties of ΔZ in quadrature through the calculation of t. For the Western transect we used the following mean values: $\Delta Z = 870 \pm 90$ m and $E = 1071 \pm 321$ m/Ma (2σ, $N = 3$). For the Central transect we used the following mean values: $\Delta Z = 748 \pm 56$ m and $E = 823 \pm 247$ m/Ma (2σ, $N = 4$). For the Eastern transect we used the following mean values: $\Delta Z = 748 \pm 56$ m and $E = 957 \pm 287$ m/Ma (2σ, $N = 3$). With these estimates, equation (8) yields durations of surface uplift of ~0.81 ± 0.29 Ma (2σ), 0.91 ± 0.29 Ma (2σ), and 0.78 ± 0.27 Ma (2σ) for the Western, Central, and Eastern transects, respectively, with a mean value of 0.8 Ma. Because the rate of incision into bedrock at the position of the convex knickpoint was likely nonzero early in the period of surface uplift (before the onset of local aggradation), our calculations will likely somewhat underestimate the duration of surface uplift. Because of this underestimation, we suggest a more conservative intiation of surface uplift to be in the last 1 Myr.

One caveat of this calculation is the assumption that our cosmogenic radionuclide erosion rates from plausibly steady state catchments (i.e., those not isolated from baselevel fall by major convex knickpoints on low-relief surfaces) reflect uplift rates that have been steady since the timing of surface uplift initiation, or the past ~1 Ma. Our topographic analysis and careful selection of basins—all those in critical landscape positions to constrain the uplift history have smooth concave profiles well described by a uniform channel steepness (k_{sn}) —strongly supports the interpretation that these landscapes are now in steady state (erosion rates balance rock uplift rates), and that rock uplift rates have been steady over the past 1–2 Ma given the response time of landscape adjustment [*Whipple*, 2001; *Whipple and Meade*, 2006]. It has also been demonstrated that cosmogenic nuclide erosion rates track well with independently measured estimates of rock uplift or longer-term erosion rates in numerous landscapes [*Cyr and Granger*, 2008; *Matmon et al.*, 2003; *Ouimet et al.*, 2009; *Wittmann et al.*, 2007]. Similarly, modeled erosion rates from low-temperature thermochronometers averaged over the Quaternary yield similar values as nearby basin-averaged erosion rates within the Mangde and Kuri Chu valleys, ~100–300 m/Ma [*Adams et al.*, 2015], upstream of the proposed duplex. Moreover, *Adams et al.* [2015] suggested that the thermochronometric data could also permit an increase in erosion rate (up to ~1000 m/Ma) during the Quaternary, provided this acceleration took place no earlier than 1.75 Ma. The consistency between the rates and timing implied by the detrital CRN erosion rates and the low-temperature thermochronometric constraints on exhumation rates supports the interpretation that the cosmogenic erosion rates are indeed quantitatively reflective of long-term erosion rates.

8. Synthesis and Discussion

8.1. Mecahnisms of In Situ Production of Low Relief

There has been a disconnect in Bhutan among (1) the temporal constraints of long-lived tectonic processes measured with geo- and thermochronometric data; (2) the more recent landscape response to tectonic and climatic processes, which are too recent to be detected with these techniques; and (3) the modern deformation field that can be measured using geodetic methods. In this study, we have attempted to bridge these gaps in order to develop a more complete picture of the evolution of the Bhutan Himalaya, and we suggest that there is a common history to all available data. Analyses of geochronometric and thermochronometric data have led past authors to suggest that shortening across Bhutan decreased secularly after the late Miocene due to the partitioning of slip between Himalayan and Shillong Plateau structures in the Miocene [*Long et al.*, 2012; *Coutand et al.*, 2014; *Adams et al.*, 2015]. As described in *Adams et al.* [2015], the effect of this decrease would manifest as a wearing down of the Eastern Himalaya—a reduction in mean elevation, relief, and taper of the range. Nonetheless, geomorphic evidence for recent surface uplift in the Bhutanese hinterland requires a more complex tectonic scenario than that suggested by thermochronometric data alone. Indeed, if the shortening rates across the Bhutan Himalaya were once again increased (e.g., fast GPS shortening rates [*Banerjee et al.*, 2008; *Vernant et al.*, 2014]), after initiation of the Shillong Plateau structures, then the Himalayan range would need to return to a higher relief state and a higher taper angle. Increasing the taper of an orogen could be accommodated by duplexes in the hinterland [e.g., *Robinson et al.*, 2003; *DeCelles et al.*, 1995; *Erickson et al.*, 2001; *Mitra and Sussman*, 1997; *Ferrill and Dunne*, 1989]. As such, this young duplex deformation may be associated with a structural adjustment within the Himalaya after returning to higher shortening rates from an earlier (late Miocene-Pliocene) period of reduced shortening rates.

Many previous authors have used the balanced cross sections across Bhutan to infer subsurface structure [*Bhargava*, 1995; *McQuarrie et al.*, 2008; *Long et al.*, 2011; *Tobgay et al.*, 2012], while others have inverted erosion

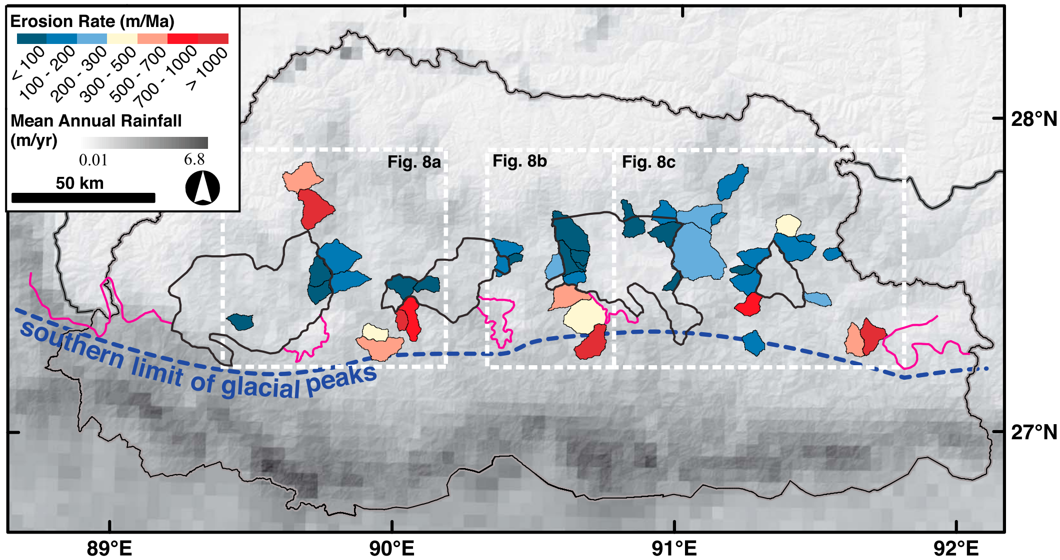

Figure 7. Map of 12 year average, mean annual rainfall derived from Tropical Rainfall Measurement Mission 2B31 data set [*Bookhagen and Burbank*, 2010], and basin-averaged erosion rates in Bhutan. Low-relief fluvial landscapes are outlined in black lines. Outliers of glacial terrains are outlined with magenta lines. Dashed white boxes show the extent of transects in Figure 8. Note the high erosion rates in line with the high glacial landscapes. Low-relief landscapes are dominated by very low erosion rates.

rate data in an attempt to constrain fault geometries [*Robert et al.*, 2011; *Coutand et al.*, 2014; *Le Roux-Mallouf et al.*, 2015]. There is, however, little agreement on the geometry of the sole thrust of the Bhutan Himalaya. The work of *Long et al.* [2011] and *Tobgay et al.* [2012] suggested that the size and position of exhumed and blind duplex structures are variable in size and geographic location across Bhutan, and the geometries of these structures are required to balance cross sections, but are not unique solutions. 2-D models used to invert erosion rates [*Robert et al.*, 2011; *Coutand et al.*, 2014; *Le Roux-Mallouf et al.*, 2015] are limited due to their assumption of steady state topography, which we have demonstrated here and in a previous paper [*Adams et al.*, 2013] to be false. Furthermore, these models assume that the only two free variables controlling surface erosion rates are the geometry of the sole thrust and the velocity of the upper plate, implying a complete lack of upper plate deformation (no duplex growth or out-of-sequence faulting). Our analysis recognizes and exploits the disequilibrium between rock uplift rate and erosion rate evident in Bhutan to derive a more robust estimate of temporal and spatial variability in rock uplift rate independent of limited constraints on the geometry of the sole thrust. Indeed, our estimate of the rock uplift rate at the crest of our inferred antiformal uplift (~1 mm/yr) suggests that no more than 1.5–3 mm/yr of horizontal shortening is absorbed on fault ramps within the growing antiformal stack, assuming ramp dips from 15 to 30°. The degree to which we can compare our findings to balanced cross sections and geophysical imaging of the sole thrust is limited by the fact that the dramatic re-structuring of the topography observed in Bhutan involves only ~1 km of rock uplift, well below the resolution of available balanced cross sections and knowledge of sole thrust geometry [e.g., *Robert et al.*, 2011; *Coutand et al.*, 2014].

Another mechanism for producing elevated, low-relief landscapes was recently proposed by *Yang et al.* [2015], whereby river capture events can create beheaded catchments with greatly reduced erosional capacity, leading to net surface uplift in response to a reduction in erosion rate. This mechanism fails in Bhutan for two primary reasons. First, according to the river capture hypothesis, relief and erosion rate reductions occur in response to reduced drainage areas. As erosion rate is proportional to A^{m_b} (equation (4)), the factor of ~10 reduction from high rates in deep canyons to low rates on the low-relief landscapes in Bhutan would require a factor of 10–100 reduction in drainage area (for $0.5 \leq m_b \leq 1$ as commonly assumed). Allowing for paleo-basins 10 to 100 times larger for even a fraction of the low-relief surfaces, nevermind all of them, is not plausible in Bhutan. Second, χ plots of the rivers draining low-relief landscapes show that they are shifted above the regional mean (Figures 3 and S1), which *Yang et al.* [2015] and *Willett et al.* [2014] would interpret as a signal of a drainage area *increase*, opposite that expected for the drainage capture mechanism. Moreover, our erosion rate data clearly show that these basins are losing area to adjacent basins with higher erosion rates. The high-elevation, low-relief landscapes in Bhutan are therefore incompatible with the drainage capture hypothesis of *Yang et al.* [2015].

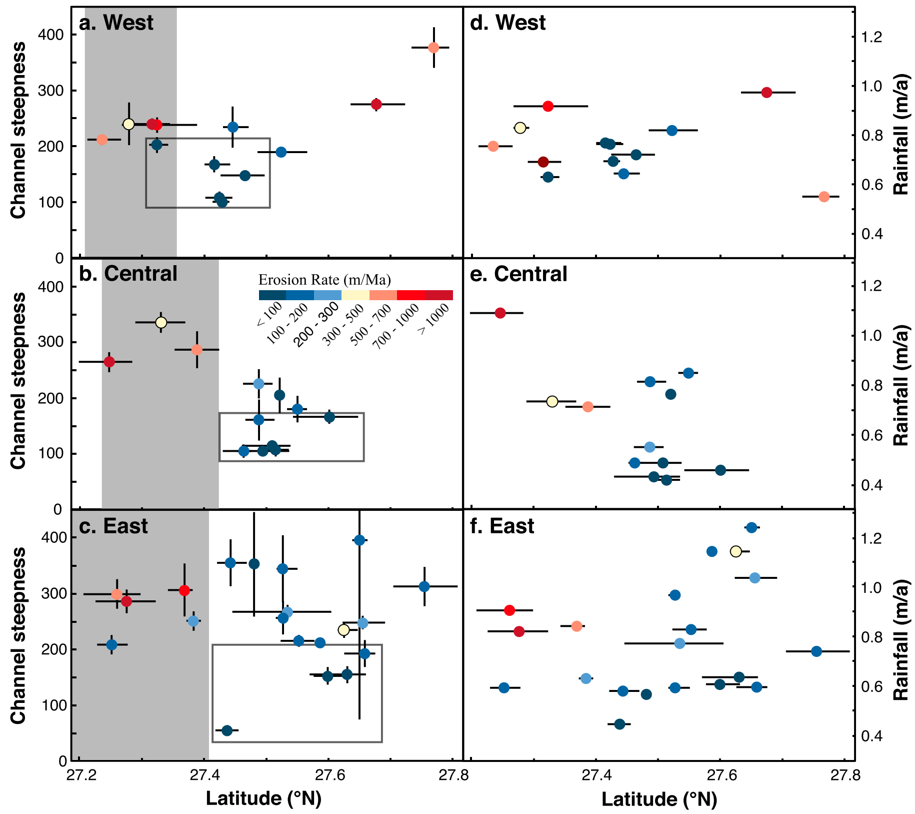

Figure 8. Basin-averaged erosion rates from three transects in Bhutan. See Figure 7 for locations. (a–c) Basins are plotted by the mean channel steepness of each basin (ordinate; error bars are 2 standard errors), the mean latitude (abscissa; error bars denote latitude range), and erosion rate (color). Vertical gray bars mark the latitudes of glacial terrain in each transect. Black boxes denote samples from low-relief landscapes. The weaker correlation between channel steepness and erosion rate in Figure 8c may be caused by minor knickpoints not identified before sampling (see Figure S3). (d–f) Basins are plotted by the mean annual rainfall from Tropical Rainfall Measurement Mission data [*Bookhagen and Burbank*, 2010].

8.2. Analysis of Landscape Evolution Model Results

The results from our landscape evolution experiments suggest that even a small, active duplex can dramatically change the surface cover (e.g., alluvial and colluvial sediments, and bedrock) and topography of a mountain range. We designed these experiments with two important boundary conditions. (1) The sediment transport coefficient was higher than the bedrock erodibility coefficient. This relationship is observed in Bhutan where channel steepness values decrease dramatically downstream across PT_2 as fluvial processes transition from detachment- to transport-limited. (2) The uplift at the crest of the duplex was higher than the uplift rates at the ends of the limbs. This pattern is also observed in Bhutan as evident from our CRN erosion rate map (Figure 7). The flexibility of our models to allow river reaches to be either transport- or detachment-limited depending on the circumstances changed the relief structure spatially and temporally within the experimental landscape. The ratio of uplift rates set the equivalent of a rotational velocity of the back tilting in the back limb of the duplex. This uplift rate ratio ($U_h/U_l \approx 4$) was required in our simulations to create a knickpoint that moved slowly enough to allow low-relief landscapes to form upstream but ensure that rivers were not completely defeated.

Beyond the initial testing to ensure low-relief landscapes were formed, subsequent adjustments to these boundary conditions modified the landscape response time and the scale of topographic parameters, but not the fundamental pattern of landscape response, which is the most meaningful result of our simulations. We adopted a symmetrical pattern of antiformal rock uplift for simplicity, but our main interpretations of landscape response are not contingent on this specific geometry. Indeed, the most important forcing factor within our models is the rock uplift rate gradient represented by the back limb of our modeled duplex, as this created the fluvial dynamics responsible for creating elevated, low-relief landscapes. A critical finding of these

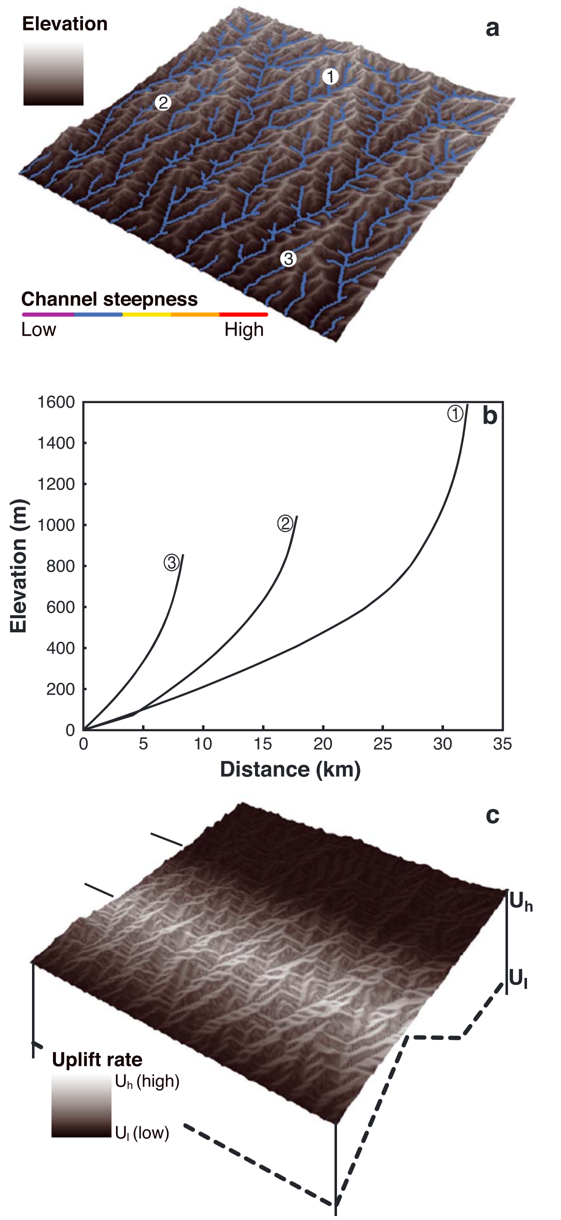

Figure 9. (a) Initial steady state topography created using the CHILD landscape evolution model with a uniform uplift rate. Erosion rate and channel steepness values are equal in all parts of the landscape. (b) Longitudinal profiles of rivers from the initial steady state landscape. Numbers mark the locations of basins in Figure 9b. (c) Map of the rock uplift rate gradient later imposed on the initial steady state landscape. Cross section shows the shape of the uplift rate function. U_h, high uplift rate at the crest of the duplex; U_l, low uplift rate at the base of the duplex.

observations and experiments is that patterns of topography, erosion, and deposition in Bhutan signify that back-tilting has occurred in the middle latitudes between the southern glacial peaks and south of PT_2. As our analyses do not extend all the way to the range front, our findings do not rule out an asymmetrical rock uplift pattern. A combination of the oversteepening of major rivers draining the low-relief landscape patches, possibly due to the reduction of gravels transported across convex knickpoints, and plausible increases in erosional efficiency (higher precipitation rates and arguably more erodible rocks) at the range front would influence the uplift pattern required to explain the topography between the southern edge of the low-relief surfaces and the range front.

By design, all drainages that crossed the active duplex in our experiments developed large convex knickpoints and the upper portions of the drainage appeared to be at least temporarily disconnected from the baselevel of the entire fluvial system by an extremely steep reach of the river (Figure 10f). This quasi-hanging valley topography was created by the selection of the uplift rate within the duplex. It was necessary to select a large uplift ratio because the basic rules for sediment transport and river incision (i.e., equations (4) and (5)) did not provide an adequate mechanism for the creation of hanging valleys in our model. Consequently, a lower uplift rate could have created hanging valleys in a model that includes a sediment-flux dependence on river incision (i.e., the tools and cover effects) [*Gasparini et al.*, 2007; *Crosby et al.*, 2007]. *Whipple and Gasparini* [2014] suggested a simple metric to consider the likelihood of creating a hanging valley. They find that, in general, the critical rock uplift rate (U_{cr}) required to create a hanging valley of a certain total drainage area (A) is dependent on the fraction of sediment passed over the knickpoint in the form of gravel (β, dimensionless), where $U_{cr} \propto (\beta A)^{1/2}$. The form of this relationship shows that lower rock uplift rates can form hanging valleys as fewer gravels are transported across the knickpoint (i.e., as β tends toward zero). This relationship could explain why not all N-S trending rivers in Bhutan that cross the blind duplexes form elevated, low-relief landscapes (Figure 2b). Indeed, smaller basins (e.g., those of the Phobjikha and Yarab surfaces) could readily become hanging valleys, but slight differences in gravel transportation could also create hanging valleys in larger basins (e.g., the Thimpu and Bumthang surfaces). The oversteepened river reaches downstream of the large convex knickpoints

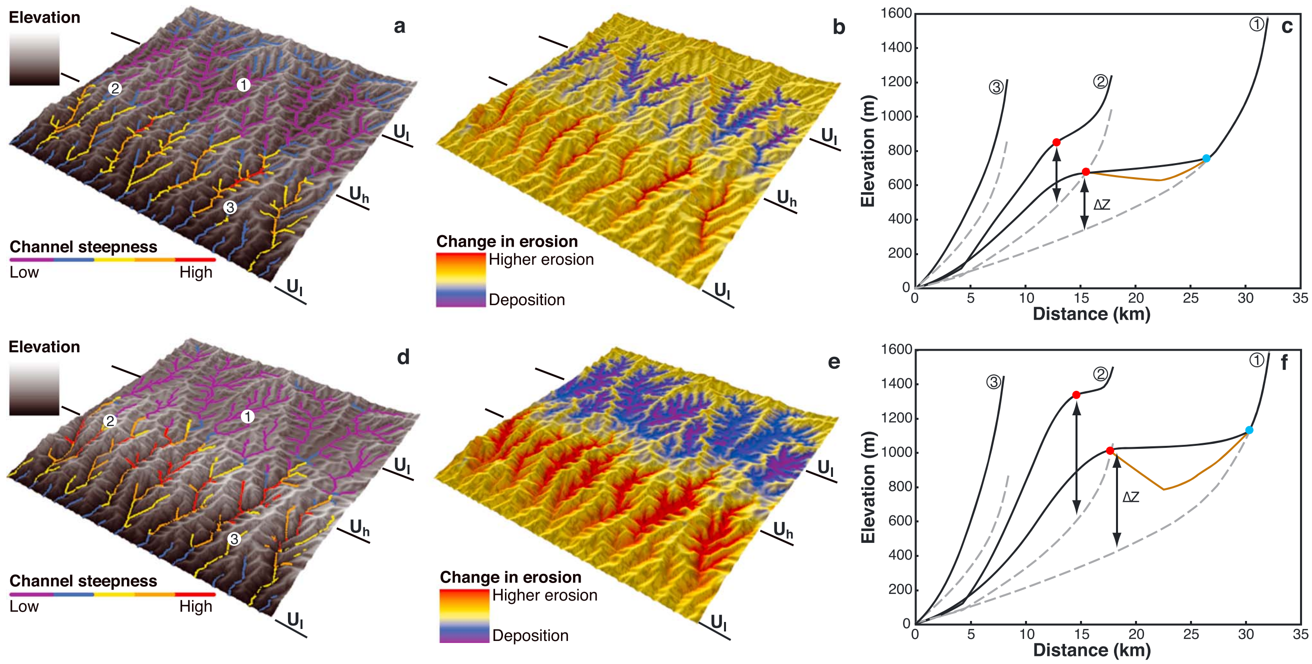

Figure 10. (a and d) Transient topographies created using the CHILD landscape evolution model after initial, and further response to an active duplex. River channels are colored by channel steepness. (b and e) Erosion rate maps created after initial, and further response to an active duplex. Color ramps are in reference to initial steady erosion rate (e.g., portions of the landscape eroding at the initial rate are in yellow). (c and f) Longitudinal profiles created after initial, and further response to an active duplex. Red dots mark the locations of transient convex knickpoints. Numbers mark the locations of basins in Figures 10c and 10f. Blue dots mark the location of transient concave knickpoints and the juxtaposition of terrains similar to Physiographic Transition 2 in Bhutan. The dashed lines represent the initial profiles of steady state rivers (Figure 9b). The magnitude of surface uplift (ΔZ) at each time step can be measured directly. Lines mark the positions of changes in the rock uplift rate gradient seen in Figure 9c. Brown lines show the depth to bedrock and thus the depth of sediment deposits. U_h, high uplift rate of at the crest of the duplex, U_l, low uplift rate at the base of the duplex.

in Bhutan, which are on average three times steeper than adjacent basins and trunk streams (Figure S1), suggest that the migration of these knickpoints is being retarded by the lack of tools needed to incise into bedrock. This affect could also allow for the production of low-relief landscapes from a more subtle backtiliting (i.e., lower rock uplift rate ratio). The reduction in gravel transport may be as important in the creation and preservation of the elevated, low-relief landscapes in Bhutan as the nonuniform rock uplift pattern. However, a mechanism for changes in rock uplift rate and/or the transportation of gravel is still required.

Importantly, we note that all major river systems in Bhutan do contain some portion of the low-relief landscapes (Figure 2b), if only in the headwaters of smaller tributaries. The Thimpu surface is completely contained within the Wang Chu drainage. Portions of the Phobjikha surface are located in the Puna Tsang Chu and Mangde Chu drainages. Portions of the Bumthang surface are located in the Mangde Chu, Chamkhar Chu, and Kuri Chu drainages. This observation makes it clear that while some trunk rivers were able to adjust to back-tilting and avoid significant aggradation, these drainage systems did experience this forcing and not all tributaries were able to keep up with the trunk river. In addition, aggraded sections of the Puna Tsang Chu and Kulong Chu (Figure 4) that appear as low channel steepness reaches in Figure 3 are located at the same latitudes as the elevated, low-relief landscapes, and may be further evidence that large, deeply incised streams struggle to keep up with an impinging zone of higher rock uplift rates.

Despite the simplicity of our landscape evolution model, the results of our experiments provide a useful guide to the interpretation of the low-relief landscapes of Bhutan. Our experiment confirmed that a hinterland duplex would create actively infilling and uplifting intermontane basins. There are many examples of similar processes occurring near the foreland of the Himalaya where actively growing antiforms impede drainages, and form sediment filled intermontane basins [e.g., *Valdiya*, 1993]. Among these examples, is the spectacular and well-known Kathmandu Basin [e.g., *Valdiya*, 1993], which has at times been the site of shallow lakes and low-gradient rivers from the Pliocene through the Quaternary [e.g., *Dill et al.*, 2003]. The many generations of lacustrine and alluvial and colluvial fills have dramatically reduced the local relief in this portion of the Central Nepal Himalaya.

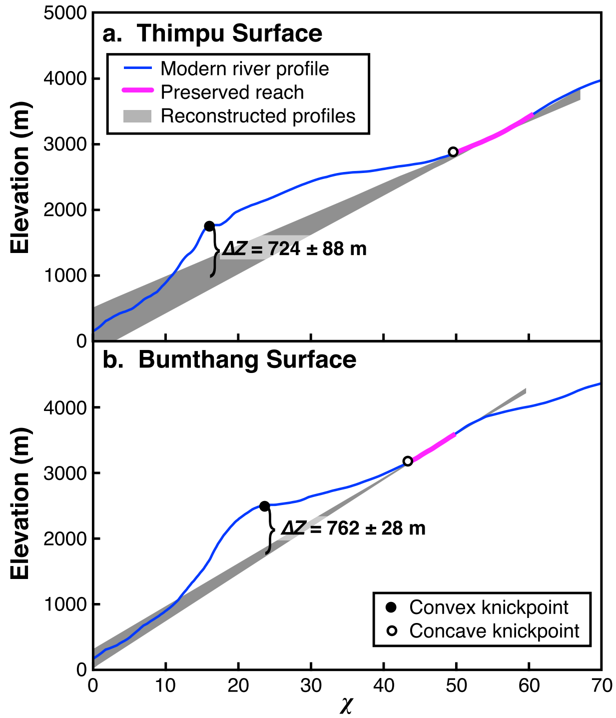

Figure 11. Example paleo-river profile reconstructions from the (a) Thimpu and (b) Bumthang surfaces. Blue solid lines are the modern linearized profiles (see text for discussion). The gray envelope shows the range of 10,000 extrapolated linearized profiles of the preserved reaches (magenta lines). Surface uplift magnitudes (ΔZ) are reported as the mean and 2 standard deviations of the 10,000 regression results.

Our landscape evolution experiment also supports the hypothesis that such low-relief landscapes are transient features whose positions are controlled by headward migrating, convex knickpoints, as evident from the dichotomy in erosion rates between the low-relief landscapes and adjacent canyons. Most importantly, we found that these low-relief landscapes could be formed in situ during uplift (Figure 6). This point leads us to an important new interpretation: that Bhutan's low-relief landscapes did not form a terrain analogous to the foothills of the central Himalaya, despite the similarity in topographic character.

Our experiments also provide interesting insight into the formation of PT_2 in Bhutan. A break in local relief and mean elevation formed upstream of the duplex in our experiment. Mountain peaks upstream of the duplex continued to erode, but the resulting sediments were stored locally in broad alluvial valleys because of the impinging zone of high rock uplift rate downstream. The results of our experiments suggest that the boundary of deposition and relief reduction migrates headward and that the strength of this signal as detected in the local relief decreases as a function of time. If PT_2 in Bhutan was formed by a similar mechanism, it is a transient landform whose position is dictated by the migration of a concave knickpoint at the northern edge of the low-relief landscapes, and not a fault. While *Adams et al.* [2013] did note a correlation of PT_2 and the Lhuentse fault, they concluded that the kinematics of the fault were not suggestive of a causative mechanism for uplift of the physiographic higher Himalaya relative to the regions to the south. However, the correlation of PT_2 and the Lhuentse fault might be expected if both were formed near the northern edge of an active blind duplex, assuming the fault marks the hinterland extent of active duplex deformation [*Adams et al.*, 2013], and the zone of aggradation caused by duplex deformation and back tilting also reaches this position. In addition, the timing of surface uplift is interesting as it is around the same time that *Adams et al.* [2013] suggested that the Lhuentse fault was likely active (Quaternary).

9. Conclusion

The variability in the surface deposits, fluvial transport state, and mean elevation across the Bhutan Himalaya suggests a dynamic landscape incompatible with either simple foreland-propagating faulting or climate change independent of tectonic adjustments. We show that (1) the creation of high-elevation, low-relief landscapes covered by thick packages of sediment accumulation, (2) the chain of high, glaciated peaks along their southern margins, and (3) the enigmatic physiographic transition that marks their northern boundaries can be explained by landscape response to a complex rock uplift rate pattern, which could be created by an active blind duplex. To explore the plausibility of this hypothesis we utilized a landscape evolution model and demonstrated that landscapes with similar patterns of topography and erosion rate are readily formed when imposing a nonuniform rock uplift pattern where rates are higher in downstream portions of the landscape.

A similar uplift pattern in Bhutan is supported by the spatial pattern of basin-averaged cosmogenic radionuclide erosion rates. These erosion rates also revealed that the low-relief landscapes are, in fact, transient and undergoing surface uplift, as surmised in analysis of river profiles and local relief. We exploited preserved reaches of rivers that did not experience syn-surface uplift, deposition, or glacial incision, to reconstruct river profiles that are representative of the form of landscapes before recent duplex deformation. Using these paleo-river profiles we calculated the surface uplift magnitude associated with the creation of the low-relief landscapes in Bhutan, resulting in ~800 m of surface uplift. With the magnitude of surface uplift constrained, we used estimates of the current rock uplift rates from our basin-averaged erosion rates to find that surface uplift was initiated ~0.8–1 Ma before the present. The recent activation of a duplex in the hinterland of the Bhutan Himalaya may suggest the range is adjusting to increase its relief and taper after a protracted period of decreased fault slip rates due to the development of the Shillong Plateau to the south during the Miocene.

Acknowledgments
We dedicate this paper to Kurt Frankel. Kurt was an excellent example of stewardship in our scientific community, and an even better friend. Without him this research would not have been possible. The research in this paper was supported by a National Science Foundation Tectonics Program grant EAR 0708714 to K.V.H. and a joint Tectonics and Geomorphology and Landuse Dynamics Programs grant EAR 1049888 to K.X.W. and A.M.H. B.A.A. is grateful for the efforts of Frances Cooper (University of Bristol) in both the field and at the drawing board. We also thank Brian Yanites (University of Idaho) and Nicole Gasparini (Tulane University) for their assistance getting CHILD operational. Fieldwork would not have been possible without support of our friends and colleagues in Bhutan: Peldon Tshering (National Environment Commission), Ugyen Wanda (Department of Geology and Mines), Karma Choden, and Ugyen Rinzen (Yangphel Adventure Travel). We are grateful for the editorial assistance of John Buffington and Jon Pelletier. This manuscript was greatly improved by reviews from Dirk Scherler, Bodo Bookhagen, John Buffington, Jon Pelletier, and an anonymous reviewer. All analytical data used in this study are provided in Excel format in the supporting information. For other data requests, please contact the corresponding author at Byron.Adams@uni-tuebingen.de

References

Adams, B. A., K. V. Hodges, M. C. van Soest, and K. X. Whipple (2013), Evidence for Pliocene-Quaternary normal faulting in the hinterland of the Bhutan Himalaya, *Lithosphere*, *5*(4), 438–449, doi:10.1130/l277.1.

Adams, B. A., K. V. Hodges, K. X. Whipple, T. A. Ehlers, M. C. van Soest, and J. Wartho (2015), Constraints on the tectonic and landscape evolution of the Bhutan Himalaya from thermochronometry, *Tectonics*, *34*, 1329–1347, doi:10.1002/2015TC003853.

Baillie, I. C., and C. Norbu (2004), Climate and other factors in the development of river and interfluve profiles in Bhutan, Eastern Himalayas, *J. Asian Earth Sci.*, *22*(5), 539–553, doi:10.1016/s1367-9120(03)00092-0.

Baillie, I. C., K. Tshering, T. Dorji, H. B. Tamang, C. Norbu, A. A. Hutcheon, and R. Baumler (2004), Regolith and soils in Bhutan, Eastern Himalayas, *Eur. J. Soil Sci.*, *55*(1), 9–27, doi:10.1046/j.1365-2389.2003.00579.x.

Balco, G., J. O. Stone, N. A. Lifton, and T. J. Dunai (2008), A complete and easily accessible means of calculating surface exposure ages or erosion rates from (10)Be and (26)Al measurements, *Quat. Geochronol.*, *3*(3), 174–195, doi:10.1016/j.quageo.2007.12.001.

Banerjee, P., R. Burgmann, B. Nagarajan, and E. Apel (2008), Intraplate deformation of the Indian subcontinent, *Geophys. Res. Lett.*, *35*, L18301, doi:10.1029/2008GL035468.

Bhargava, O. (1995), *The Bhutan Himalaya, A Geological Account*, Geological Survey of India, Calcutta.

Bierman, P., and E. J. Steig (1996), Estimating rates of denudation using cosmogenic isotope abundances in sediment, *Earth Surf. Processes Landforms*, *21*(2), 125–139, doi:10.1002/(sici)1096-9837(199602)21:2<125::aid-esp511>3.0.co;2-8.

Bookhagen, B., and D. W. Burbank (2010), Toward a complete Himalayan hydrological budget: Spatiotemporal distribution of snowmelt and rainfall and their impact on river discharge, *J. Geophys. Res.*, *115*, F03019, doi:10.1029/2009JF001426.

Boyer, S. E., and D. Elliott (1982), Thrust systems, *AAPG Bull.*, *66*(9), 1196–1230.

Brozović, N., D. W. Burbank, and A. J. Meigs (1997), Climatic limits on landscape development in the northwestern Himalaya, *Science*, *276*(5312), 571–574.

Burbank, D., A. Meigs, and N. Brozović (1996), Interactions of growing folds and coeval depositional systems, *Basin Res.*, *8*(3), 199–223, doi:10.1046/j.1365-2117.1996.00181.x.

Chambers, J., R. Parrish, T. Argles, N. Harris, and M. Horstwood (2011), A short duration pulse of ductile normal shear on the outer South Tibetan detachment in Bhutan: Alternating channel flow and critical taper mechanics of the eastern Himalaya, *Tectonics*, *30*, TC2005, doi:10.1029/2010TC002784.

Coutand, I., D. M. Whipp, D. Grujic, M. Bernet, M. G. Fellin, B. Bookhagen, K. R. Landry, S. Ghalley, and C. Duncan (2014), Geometry and kinematics of the Main Himalayan Thrust and Neogene crustal exhumation in the Bhutanese Himalaya derived from inversion of multi-thermochronologic data, *J. Geophys. Res. Solid Earth*, *119*, 1446–1481, doi:10.1002/2013JB010891.

Crosby, B. T., K. X. Whipple, N. M. Gasparini, and C. W. Wobus (2007), Formation of fluvial hanging valleys: Theory and simulation, *J. Geophys. Res.*, *112*, F03S10, doi:10.1029/2006JF000566.

Cyr, A. J., and D. E. Granger (2008), Dynamic equilibrium among erosion, river incision, and coastal uplift in the northern and central Apennines, Italy, *Geology*, *36*(2), 103–106.

Daniel, C., L. Hollister, R. T. Parrish, and D. Grujic (2003), Exhumation of the Main Central thrust from lower crustal depths, eastern Bhutan Himalaya, *J. Metamorph. Geol.*, *21*(4), 317–334.

Davis, D., J. Suppe, and F. A. Dahlen (1983), Mechanic of fold-and-thrust belts and accretionary wedges, *J. Geophys. Res.*, *88*(NB2), 1153–1172, doi:10.1029/JB088iB02p01153.

Decelles, P. G., T. F. Lawton, and G. Mitra (1995), Thrust timing, growth of structural culminations, and synorogenic sedimentation in the type Sevier Orogenic Belt, western United-States, *Geology*, *23*(8), 699–702, doi:10.1130/0091-7613(1995)023<0699:ttgosc>2.3.co;2.

DiBiase, R. A., K. X. Whipple, A. M. Heimsath, and W. B. Ouimet (2010), Landscape form and millennial erosion rates in the San Gabriel Mountains, CA, *Earth Planet. Sci. Lett.*, *289*(1), 134–144.

Dill, H. G., D. R. Khadka, R. Khanal, R. Dohrmann, F. Melcher, and K. Busch (2003), Infilling of the Younger Kathmandu-Banepa intermontane lake basin during the Late Quaternary (Lesser Himalaya, Nepal): A sedimentological study, *J. Quat. Sci.*, *18*(1), 41–60, doi:10.1002/jqs.726.

Duncan, C., J. Masek, and E. Fielding (2003), How steep are the Himalaya? Characteristics and implications of along-strike topographic variations, *Geology*, *31*(1), 75–78.

Erickson, S. G., L. M. Strayer, and J. Suppe (2001), Initiation and reactivation of faults during movement over a thrust-fault ramp: Numerical mechanical models, *J. Struct. Geol.*, *23*(1), 11–23, doi:10.1016/s0191-8141(00)00074-2.

Ferrill, D. A., and W. M. Dunne (1989), Cover deformation above a blind duplex: An example from West-Virginia, USA, *J. Struct. Geol.*, *11*(4), 421–431, doi:10.1016/0191-8141(89)90019-9.

Flint, J. (1974), Stream gradient as a function of order, magnitude, and discharge, *Water Resour. Res.*, *10*(5), 969–973.

Gansser, A. (1983), *Geology of the Bhutan Himalaya*, 181 pp., Birkhäuser Verlag, Basel.

Gasparini, N. M., K. X. Whipple, and R. L. Bras (2007), Predictions of steady state and transient landscape morphology using sediment-flux-dependent river incision models, *J. Geophys. Res.*, *112*, F03S09, doi:10.1029/2006JF000567.

Granger, D. E., J. W. Kirchner, and R. Finkel (1996), Spatially averaged long-term erosion rates measured from in situ-produced cosmogenic nuclides in alluvial sediment, *J. Geol.*, *104*(3), 249–257.

Grujic, D., M. Casey, C. Davidson, L. S. Hollister, R. Kündig, T. Pavlis, and S. Schmid (1996), Ductile extrusion of the Higher Himalayan Crystalline in Bhutan: Evidence from quartz microfabrics, *Tectonophysics*, *260*(1), 21–43.

Grujic, D., L. S. Hollister, and R. R. Parrish (2002), Himalayan metamorphic sequence as an orogenic channel: Insight from Bhutan, *Earth Planet. Sci. Lett.*, *198*(1), 177–191.

Grujic, D., I. Coutand, B. Bookhagen, S. Bonnet, A. Blythe, and C. Duncan (2006), Climatic forcing of erosion, landscape, and tectonics in the Bhutan Himalayas, *Geology*, *34*(10), 801–804, doi:10.1130/g22648.1.

Hack, J. T. (1957), *Studies of Longitudinal Stream Profiles in Virginia and Maryland*, *U.S. Geol. Surv. Prof. Pap.*, *294*, 97 pp., Reston, Va.

Heim, A., and A. Gansser (1939), *Central Himalaya: Geological Observations of the Swiss Expedition 1936*, 245 pp., Mémoires de la Société Helvétique des Sciences Naturelles, Zurich.

Heisinger, B., D. Lal, A. J. T. Jull, P. Kubik, S. Ivy-Ochs, K. Knie, and E. Nolte (2002a), Production of selected cosmogenic radionuclides by muons: 2. Capture of negative muons, *Earth Planet. Sci. Lett.*, *200*(3–4), 357–369.

Heisinger, B., D. Lal, A. J. T. Jull, P. Kubik, S. Ivy-Ochs, S. Neumaier, K. Knie, V. Lazarev, and E. Nolte (2002b), Production of selected cosmogenic radionuclides by muons 1. Fast muons, *Earth Planet. Sci. Lett.*, *200*(3–4), 345–355, doi:10.1016/s0012-821x(02)00640-4.

Hodges, K. V., and B. A. Adams (2013), The influence of middle and lower crustal flow on the landscape evolution of orogenic plateaus: Insights from the Himalaya and Tibet, in *Treatise on Geomorphology*, edited by L. Owen, Academic Press, San Diego, Calif.

Hodges, K. V., J. M. Hurtado, and K. X. Whipple (2001), Southward extrusion of Tibetan crust and its effect on Himalayan tectonics, *Tectonics*, *20*(6), 799–809.

Hodges, K. V., C. Wobus, K. Ruhl, T. Schildgen, and K. Whipple (2004), Quaternary deformation, river steepening, and heavy precipitation at the front of the Higher Himalayan ranges, *Earth Planet. Sci. Lett.*, *220*(3), 379–389.

Howard, A. D., and G. Kerby (1983), Channel changes in badlands, *Geol. Soc. Am. Bull.*, *94*(6), 739–752.

Humphrey, N. F., and S. K. Konrad (2000), River incision or diversion in response to bedrock uplift, *Geology*, *28*(1), 43–46, doi:10.1130/0091-7613(2000)28<43:riodir>2.0.co;2.

Iwata, S., C. Narama, and Karma (2002), Three Holocene and late Pleistocene glacial stages inferred from moraines in the Lingshi and Thanza village areas, Bhutan, *Quat. Int.*, *97–8*, 69–78, doi:10.1016/s1040-6182(02)00052-6.

Kober, F., K. Hippe, B. Salcher, S. Ivy-Ochs, P. Kubik, L. Wacker, and N. Hählen (2012), Debris-flow–dependent variation of cosmogenically derived catchment-wide denudation rates, *Geology*, *40*(10), 935–938.

Lal, D. (1991), Cosmic-ray labeling of erosion surfaces – insitu nuclide production-rates and erosion models, *Earth Planet. Sci. Lett.*, *104*(2–4), 424–439, doi:10.1016/0012-821x(91)90220-c.

Lave, J., and J. P. Avouac (2000), Active folding of fluvial terraces across the Siwaliks Hills, Himalayas of central Nepal, *J. Geophys. Res.*, *105*(B3), 5735–5770, doi:10.1029/1999JB900292.

Le Roux-Mallouf, R., V. Godard, R. Cattin, M. Ferry, J. Gyeltshen, J. F. Ritz, D. Drupka, V. Guillou, M. Arnold, and G. Aumaître (2015), Evidence for a wide and gently dipping Main Himalayan Thrust in western Bhutan, *Geophys. Res. Lett.*, *42*, 3257–3265, doi:10.1002/2015GL063767.

Long, S., N. McQuarrie, T. Tobgay, and D. Grujic (2011), Geometry and crustal shortening of the Himalayan fold-thrust belt, eastern and central Bhutan, *Geol. Soc. Am. Bull.*, *123*(7–8), 1427–1244, doi:10.1130/b30203.1.

Long, S. P., N. McQuarrie, T. Tobgay, I. Coutand, F. J. Cooper, P. W. Reiners, J. A. Wartho, and K. V. Hodges (2012), Variable shortening rates in the eastern Himalayan thrust belt, Bhutan: Insights from multiple thermochronologic and geochronologic data sets tied to kinematic reconstructions, *Tectonics*, *31*, TC5004, doi:10.1029/2012TC003155.

Lupker, M., P.-H. Blard, J. Lave, C. France-Lanord, L. Leanni, N. Puchol, J. Charreau, and D. Bourlès (2012), ^{10}Be-derived Himalayan denudation rates and sediment budgets in the Ganga basin, *Earth Planet. Sci. Lett.*, *333*, 146–156.

Matmon, A., P. Bierman, J. Larsen, S. Southworth, M. Pavich, and M. Caffee (2003), Temporally and spatially uniform rates of erosion in the southern Appalachian Great Smoky Mountains, *Geology*, *31*(2), 155–158.

McQuarrie, N., and T. A. Ehlers (2015), Influence of thrust belt geometry and shortening rate on thermochronometer cooling ages: Insights from thermokinematic and erosion modeling of the Bhutan Himalaya, *Tectonics*, *34*, 1055–1079, doi:10.1002/2014TC00378.

McQuarrie, N., D. Robinson, S. Long, T. Tobgay, D. Grujic, G. Gehrels, and M. Ducea (2008), Preliminary stratigraphic and structural architecture of Bhutan: Implications for the along strike architecture of the Himalayan system, *Earth Planet. Sci. Lett.*, *272*(1–2), 105–117, doi:10.1016/j.epsl.2008.04.030.

McQuarrie, N., T. Tobgay, S. P. Long, P. W. Reiners, and M. A. Cosca (2014), Variable exhumation rates and variable displacement rates: Documenting recent slowing of Himalayan shortening in western Bhutan, *Earth Planet. Sci. Lett.*, *386*, 161–174.

Meyer, M. C., C. C. Hofmann, A. M. D. Gemmell, E. Haslinger, H. Haeusler, and D. Wangda (2009), Holocene glacier fluctuations and migration of Neolithic yak pastoralists into the high valleys of northwest Bhutan, *Quat. Sci. Rev.*, *28*(13–14), 1217–1237, doi:10.1016/j.quascirev.2008.12.025.

Mitra, G., and A. J. Sussman (1997), Structural evolution of connecting splay duplexes and their implications for critical taper: An example based on geometry and kinematics of the Canyon Range culmination, Sevier Belt, central Utah, *J. Struct. Geol.*, *19*(3–4), 503–521, doi:10.1016/s0191-8141(96)00108-3.

Niemi, N. A., M. Oskin, D. W. Burbank, A. M. Heimsath, and E. J. Gabet (2005), Effects of bedrock landslides on cosmogenically determined erosion rates, *Earth Planet. Sci. Lett.*, *237*(3), 480–498.

Nishiizumi, K., M. Imamura, M. W. Caffee, J. R. Southon, R. C. Finkel, and J. McAninch (2007), Absolute calibration of ^{10}Be AMS standards, *Nucl. Instrum. Methods Phys. Res., Sect. B*, *258*(2), 403–413.

Ouimet, W. B., K. X. Whipple, and D. E. Granger (2009), Beyond threshold hillslopes: Channel adjustment to base-level fall in tectonically active mountain ranges, *Geology*, *37*(7), 579–582.

Perron, J. T., and L. Royden (2013), An integral approach to bedrock river profile analysis, *Earth Surf. Processes Landforms*, *38*(6), 570–576, doi:10.1002/esp.3302.

Plesch, A., J. H. Shaw, and D. Kronman (2007), Mechanics of low-relief detachment folding in the Bajiaochang field, Sichuan Basin, China, *Aapg Bull.*, *91*(11), 1559–1575, doi:10.1306/06200706072.

Portenga, E. W., and P. R. Bierman (2011), Understanding Earth's eroding surface with 10 Be, *GSA Today*, *21*(8), 4–10.

Portenga, E. W., P. R. Bierman, C. Duncan, L. B. Corbett, N. M. Kehrwald, and D. H. Rood (2015), Erosion rates of the Bhutanese Himalaya determined using in situ-produced ^{10}Be, *Geomorphology*, *233*, 112–126.

Raup, B., A. Racoviteanu, S. J. S. Khalsa, C. Helm, R. Armstrong, and Y. Arnaud (2007), The GLIMS geospatial glacier database: A new tool for studying glacier change, *Global Planet. Change*, *56*(1–2), 101–110, doi:10.1016/j.gloplacha.2006.07.018.

Robert, X., P. van der Beek, J. Braun, C. Perry, and J. L. Mugnier (2011), Control of detachment geometry on lateral variations in exhumation rates in the Himalaya: Insights from low-temperature thermochronology and numerical modeling, *J. Geophys. Res.*, *116*, B05202, doi:10.1029/2010JB007893.

Robinson, D. M., P. G. DeCelles, C. N. Garzione, O. N. Pearson, T. M. Harrison, and E. J. Catlos (2003), Kinematic model for the Main Central thrust in Nepal, *Geology*, *31*(4), 359–362.

Scherler, D., B. Bookhagen, and M. R. Strecker (2014), Tectonic control on 10Be-derived erosion rates in the Garhwal Himalaya, India, *J. Geophys. Res. Earth Surf.*, *119*, 83–105, doi:10.1002/2013JF002955.

Schoenbohm, L., K. Whipple, B. Burchfiel, and L. Chen (2004), Geomorphic constraints on surface uplift, exhumation, and plateau growth in the Red River region, Yunnan Province, China, *Geol. Soc. Am. Bull.*, *116*(7–8), 895–909.

Sobel, E. R., G. E. Hilley, and M. R. Strecker (2003), Formation of internally drained contractional basins by aridity-limited bedrock incision, *J. Geophys. Res.*, *108*(B7), 2344, doi:10.1029/2002JB001883.

Stock, J. D., and D. R. Montgomery (1999), Geologic constraints on bedrock river incision using the stream power law, *J. Geophys. Res.*, *104*(B3), 4983–4993.

Stone, J. O. (2000), Air pressure and cosmogenic isotope production, *J. Geophys. Res.*, *105*(B10), 23,753–23,759.

Stüwe, K., and D. Foster (2001), Ar-40/Ar-39, pressure, temperature and fission track constraints on the age and nature of metamorphism around the main central thrust in the eastern Bhutan Himalaya, *J. Asian Earth Sci.*, *19*(1–2), 85–95, doi:10.1016/s1367-9120(00)00018-3.

Suppe, J. (1983), Geometry and kinematics of fault-bend folding, *Am. J. Sci.*, *283*, 684–721.

Tarboton, D. G., R. L. Bras, and I. Rodriguez-Iturbe (1989), Scaling and elevation in river networks, *Water Resour. Res.*, *25*(9), 2037–2051.

Tobgay, T., N. McQuarrie, S. Long, M. J. Kohn, and S. L. Corrie (2012), The age and rate of displacement along the Main Central Thrust in the western Bhutan Himalaya, *Earth Planet. Sci. Lett.*, *319*, 146–158, doi:10.1016/j.epsl.2011.12.005.

Tucker, G., and K. Whipple (2002), Topographic outcomes predicted by stream erosion models: Sensitivity analysis and intermodel comparison, *J. Geophys. Res.*, *107*(B9), 2179, doi:10.1029/2001JB000162.

Tucker, G. E., and R. L. Bras (1998), Hillslope processes, drainage density, and landscape morphology, *Water Resour. Res.*, *34*(10), 2751–2764, doi:10.1029/98WR01474.

Tucker, G. E., S. T. Lancaster, N. M. Gasparini, R. L. Bras, and S. M. Rybarczyk (2001), An object-oriented framework for distributed hydrologic and geomorphic modeling using triangulated irregular networks, *Comput. Geosci.*, *27*(8), 959–973, doi:10.1016/s0098-3004(00)00134-5.

Valdiya, K. (1993), Uplift and geomorphic rejuvenation of the Himalaya in the Quaternary period, *Curr. Sci.*, *64*(11–12), 873–885.

Vernant, P., R. Bilham, W. Szeliga, D. Drupka, S. Kalita, A. K. Bhattacharyya, V. K. Gaur, P. Pelgay, R. Cattin, and T. Berthet (2014), Clockwise rotation of the Brahmaputra Valley relative to India: Tectonic convergence in the eastern Himalaya, Naga Hills, and Shillong Plateau, *J. Geophys. Res. Solid Earth*, *119*, 6558–6571, doi:10.1002/2014JB011196.

Wang, P., D. Scherler, J. Liu-Zeng, J. Mey, J.-P. Avouac, Y. Zhang, and D. Shi (2014), Tectonic control of Yarlung Tsangpo Gorge revealed by a buried canyon in Southern Tibet, *Science*, *346*(6212), 978–981.

Wendt, I., and C. Carl (1991), The statistical distribution of the mean squared weighted deviation, *Chem. Geol. Isot. Geosci. Sect.*, *86*(4), 275–285.

Whipple, K., and N. Gasparini (2014), Tectonic control of topography, rainfall patterns, and erosion during rapid post–12 Ma uplift of the Bolivian Andes, *Lithosphere*, *6*(4), 251–268.

Whipple, K. W. (2001), Fluvial landscape response time: How plausible is steady-state denudation?, *Am. J. Sci.*, *301*, 313–325.

Whipple, K. X. (2004), Bedrock rivers and the geomorphology of active orogens, *Annu. Rev. Earth Planet. Sci.*, *32*, 151–185, doi:10.1146/annurev.earth.32.101802.120356.

Whipple, K. X., and B. J. Meade (2006), Orogen response to changes in climatic and tectonic forcing, *Earth Planet. Sci. Lett.*, *243*(1–2), 218–228, doi:10.1016/j.epsl.2005.12.022.

Whipple, K. X., and G. E. Tucker (1999), Dynamics of the stream-power river incision model: Implications for height limits of mountain ranges, landscape response timescales, and research needs, *J. Geophys. Res.*, *104*(B8), 17,661–17,674, doi:10.1029/1999JB900120.

Whipple, K. X., and G. E. Tucker (2002), Implications of sediment-flux-dependent river incision models for landscape evolution, *J. Geophys. Res.*, *107*(B2), 2039, doi:10.1029/2000JB000044.

Whipple, K. X., E. Kirby, and S. H. Brocklehurst (1999), Geomorphic limits to climate induced increases in topographic relief, *Nature*, *401*(6748), 39–43, doi:10.1038/43375.

Willett, S. D., S. W. McCoy, J. T. Perron, L. Goren, and C.-Y. Chen (2014), Dynamic reorganization of river basins, *Science*, *343*(6175), 1,248,765, doi:10.1126/science.1248765.

Willgoose, G., R. L. Bras, and I. Rodriguez-Iturbe (1991), A coupled channel network growth and hillslope evolution model. 1. Theory, *Water Resour. Res.*, *27*(7), 1671–1684, doi:10.1029/91WR00935.

Wittmann, H., F. von Blanckenburg, T. Kruesmann, K. P. Norton, and P. W. Kubik (2007), Relation between rock uplift and denudation from cosmogenic nuclides in river sediment in the Central Alps of Switzerland, *J. Geophys. Res.*, *112*, F04010, doi:10.1029/2006JF000729.

Wobus, C. W., K. V. Hodges, and K. X. Whipple (2003), Has focused denudation sustained active thrusting at the Himalayan topographic front?, *Geology*, *31*(10), 861–864.

Wobus, C. W., K. X. Whipple, and K. V. Hodges (2006a), Neotectonics of the central Nepalese Himalaya: Constraints from geomorphology, detrital 40Ar/39Ar thermochronology, and thermal modeling, *Tectonics*, *25*, TC4011, doi:10.1029/2005TC001935.

Wobus, C., A. Heimsath, K. Whipple, and K. Hodges (2005), Active out-of-sequence thrust faulting in the central Nepalese Himalaya, *Nature*, *434*(7036), 1008–1011.

Wobus, C., K. X. Whipple, E. Kirby, N. Snyder, J. Johnson, K. Spyropolou, B. Crosby, and D. Sheehan (2006b), Tectonics from topography: Procedures, promise, and pitfalls, *Spec. Pap.-Geol. Soc. Am.*, *398*, 55–74.

Yang, R., S. D. Willett, and L. Goren (2015), In situ low-relief landscape formation as a result of river network disruption, *Nature*, *520*(7548), 526–529.

Yanites, B. J., G. E. Tucker, and R. S. Anderson (2009), Numerical and analytical models of cosmogenic radionuclide dynamics in landslide-dominated drainage basins, *J. Geophys. Res.*, *114*, F01007, doi:10.1029/2008JF001088.